SEMMELWEIS EGYETEM

DOKTORI ISKOLA

Ph.D. értekezések

3186.

CZIBOR SÁNDOR

Klinikai hematológia és infektológia

című program

Programvezető: Dr. Masszi Tamás, egyetemi tanár

Témavezetők: Dr. Györke Tamás, egyetemi docens

THE ROLE OF NUCLEAR MEDICINE IN LYMPHOMAS – A FOCUS ON PROGNOSTIC EVALUATION OF DIFFUSE LARGE B-CELL LYMPHOMA WITH POSITRON EMISSION TOMOGRAPHY

PhD thesis

Sándor Czibor

Clinical Medicine Doctoral School

Semmelweis University

Supervisor: Tamás Györke, MD, Ph.D

Official reviewers: Gergely Varga, MD, Ph.D
Zsombor Ritter MD, Ph.D

Head of the Complex Examination Committee:
Judit Demeter, MD, Ph.D

Members of the Complex Examination Committee:
Judit Müller, MD, Ph.D
Szabolcs Szakáll, MD, Ph.D

Budapest
2025

TABLE OF CONTENTS

LIST OF ABBREVIATIONS

3D: three-dimensional

41pc: 41% isocontour VOI method

aaIPI: age-adjusted IPI

ABC: activated B-cell like

ASCT: autologous stem cell transplantation

AUC: area-under-the-curve

BPL: Bayesian penalised likelihood

bwaMTV: body weight-adjusted MTV

bwaTLG: body weight-adjusted TLG

CAR: anti-CD-19 chimeric antigen receptor

CI: confidence interval

CMR: complete metabolic response

CNN: convolutional neural network

CNS: central nervous system

COO: cell of origin

CR: complete response

CSS: cause-specific survival

CT: computed tomography

DFS: disease-free survival

DICOM: Digital Imaging and Communications in Medicine

DLBCL: diffuse large B-cell lymphoma

Dmax: maximum lesion diameter

DS: Deauville-score

EANM: European Association of Nuclear Medicine

EARL: EANM Research Ltd.

ECOG: Eastern Cooperative Oncology Group

EFS: event-free survival

EoT: end of treatment

ESMO: European Society for Medical Oncology

FDG: 2-[^{18}F]fluoro-2-deoxy-D-glucose

GCB: germinal centre B cell-like

GLCM: grey-level cooccurrence matrix

GLNU: grey-level nonuniformity

glob4: >SUV4 method

GLRLM: grey-level run-length matrix

GLSZM: grey-level size zone matrix

grad: method using a gradient-based lesion growing algorithm

HL: Hodgkin's lymphoma

HR: HR: hazard ratio

I-PET: interim PET

I-PET2: interim PET performed after 2 cycles of treatment

I-PET3: interim PET performed after 3 cycles of treatment

I-PET4: interim PET performed after 4 cycles of treatment

IAEA: International Atomic Energy Agency

ICC: intraclass correlation coefficient

IMC1: informational measure of correlation

IMPI: International Metabolic Prognostic Index

IPI: International Prognostic Index

ISRT: involved site radiation therapy

LAHGLE: large area high grey-level emphasis

LASSO: least absolute shrinkage and selection operator

LDH: lactate-dehydrogenase

LZE: long-zone emphasis

LZHGE: long-zone high grey-level emphasis

LZLGE: long-zone low grey-level emphasis

mqPET: modified qPET

MRI: magnetic resonance imaging

MTV: metabolic tumour volume

NCCN-IPI: National Comprehensive Cancer Network IPI

NF-κB: nuclear factor kappa B

NGTDM: neighbourhood grey-tone difference matrix

NHL: Non-Hodgkin lymphoma

NCRI: National Cancer Research Institute

NOS: not otherwise specified

NPV: negative predictive value

OS: overall survival

OSEM: ordered subset expectation maximisation

qPET: quantitative PET

PET: positron emission tomography

PFS: progression-free survival

PG: primary gastric

PGIL: primary gastrointestinal

PPV: positive predictive value

PSF: point spread function

R-ACVBP: rituximab combined with cyclophosphamide, doxorubicin, vindesine, bleomycin, and prednisone

R-CHOP: rituximab combined with cyclophosphamide, doxorubicin, vincristine, and prednisone

R-CHP: rituximab combined with cyclophosphamide, doxorubicin, and prednisone

R-EPOCH / R-CHOEP: rituximab combined with cyclophosphamide, doxorubicin, vincristine, etoposide, and prednisone

R-IPI: revised IPI

RLNU: run length non-uniformity

ROC: receiver operating characteristics

rPET: ratio-PET

RR: resolution recovery

RS: radiomics score

SD: standard deviation

SHZGE: short-zone high grey-level emphasis

SUV: Standardised Uptake Value

SUV_{max}: maximum SUV

SUV_{mean}: mean SUV

TLG: total lesion glycolysis

TOF: time-of-flight

VOI: volume of interest

WHO: World Health Organization

1. INTRODUCTION

1.1. Diffuse large B-cell lymphoma

1.1.1. Epidemiology

Non-Hodgkin lymphoma (NHL) is the most common haematological malignancy with its global incidence comprising 2.8% of all malignant diseases (1, 2). In 2018, an estimated 509,600 new NHL cases were diagnosed in the world and its most common subtype, diffuse large B-cell lymphoma (DLBCL) accounted for 31% of all adult NHL cases in western countries (1-5).

DLBCLs are defined as a heterogeneous group of malignancies with a clonal proliferation of a germinal or post-germinal malignant B-cell (large cells with nuclei at least twice the size of a small lymphocyte and usually larger than those of tissue macrophages) that can develop at either nodal or extra-nodal sites (6, 7). Although DLBCLs manifest de novo more frequently, they may also arise from the progression or transformation of a less aggressive B-cell neoplasm, such as chronic lymphocytic leukaemia, lymphoplasmacytic lymphoma, marginal zone lymphoma or follicular lymphoma (6-8).

The aetiology of the majority of DLBCLs remains unidentified, however, some agents producing molecular aberrations (e.g. pesticides, fertilisers, and medical drugs – especially alkylating agents combined with ionizing radiation) as well as congenital and acquired immunodeficiency states are known predisposing factors (6, 9, 10).

1.1.2. Diagnosis and classification

The establishment of a diagnosis of DLBCL necessitates the histological evaluation of tissue acquired through excisional biopsy or, if alternative surgical methods are not feasible, through core biopsy with the choice of biopsy location depending on the presentation of lymphoma (6, 11). Relying solely on a fine-needle aspirate for diagnosing DLBCL is not recommended (11).

As more knowledge accumulates of NHLs, classifications are regularly revised to fit histopathological and molecular evidences, as well as clinical correlations. The patient recruitment of the studies included in the candidate's own research occurred before 2020 and to reflect the collected data, the terminology of the Revised 4th Edition of the World Health Organization (WHO) Classification of Tumours of Haematopoietic and Lymphoid Tissues is used in this present thesis and for pragmatic and didactic reasons, "DLBCL" will refer to the entity "DLBCL not otherwise specified (NOS) " in the following (7).

Different classifications of DLBCL exist, based on cell of origin, molecular features or genetic subtypes.

Cell of origin (COO) differentiates germinal centre B cell-like (GCB) and activated B-cell like (ABC) DLBCL with 10-15% of cases remaining unclassified (8, 12). The gene expression profile of GCB is characteristic of normal germinal centre B cells with intraclonal heterogeneity, ongoing somatic hypermutation, and CD10 and BCL6 expression while ABC is associated with the gene expression of post-germinal or activated B cells and is characterised by high expression and constitutive activity of the nuclear factor kappa B (NF-κB) complex and expression of IRF4 and BCL2 (8, 12).

Molecular features enabled to identify a subgroup of 8-10% of aggressive B-cell lymphoma patients who carry MYC and BCL2 and/or BCL6 rearrangements and have a worse prognosis after conventional frontline treatment – this subtype was classified as "high grade B-cell lymphoma, with MYC and BCL2 and/or BCL6 rearrangements" in the Revised 4th Edition of the WHO Classification of Tumours of Haematopoietic and Lymphoid Tissues (7, 8, 13, 14).

Utilizing whole-exome sequencing, the groups led by Schmitz, Chapuy, and Wright identified four, five, and seven genetic subtypes of DLBCL, respectively, with different prognosis (15-17).

1.1.3. Staging and risk stratification

After the diagnosis of DLBCL has been confirmed, pre-treatment evaluation and staging constitute the initial crucial phase.

Current standard staging of DLBCL utilises the Lugano modification of the system that was proposed at the Ann Arbor Conference in 1971 that includes the number of sites of involvement with their relation to the diaphragm and the presence of extranodal disease, also taking into account the presence of B symptoms as presented in Table 1 (6, 11, 18-20).

Bulky disease is defined as any nodal or extranodal tumour mass with a diameter of ≥ 7 cm (21, 22).

2-[^{18}F]fluoro-2-deoxy-D-glucose (FDG) positron emission tomography (PET) is a standard medical imaging procedure both for staging and response assessment in DLBCL and its widespread utility is detailed in later sections. For suspected central nervous system (CNS) lymphoma, magnetic resonance imaging (MRI) is the recommended imaging modality as the high physiological FDG uptake in the brain suppresses biological contrast between normal and malignant tissue on PET (11, 23). Furthermore, bone marrow biopsy, diagnostic lumbar puncture, and contrast-enhanced computed tomography (CT) may also frequently feature among staging procedures (11).

Risk stratification of DLBCL is most commonly performed according to the International Prognostic Index (IPI; Table 2) or its modifications, such as age-adjusted IPI (aaIPI), revised IPI (R-IPI) or the National Comprehensive Cancer Network IPI (NCCN-IPI) (24-29).

1.1.4. Treatment

The introduction of rituximab, a chimeric human/murine immunoglobulin G1 monoclonal antibody that binds specifically to the B-cell-surface antigen, CD20 proved to yield significant increment to overall survival in DLBCL (30).

Table 1. Staging system of DLBCL (11, 18-20)

Stage	
I	Involvement of a single lymphatic region (I) or localised involvement of single extralymphatic organ or site (IE)
II	Involvement of two or more lymphatic regions on the same side of the diaphragm (II) or localised involvement of a single extralymphatic organ or site and of one or more lymphatic regions on the same side of the diaphragm (IIE)
III	Involvement of lymphatic regions on both sides of the diaphragm
IV	Diffuse or disseminated involvement of one or more extralymphatic organs with or without lymphatic involvement
B symptoms	Fevers >38 °C for at least three consecutive days Night sweats Body weight loss >10% during the 6 months prior to diagnosis)

Currently, frontline therapy with curative intent for DLBCL is chemoimmunotherapy based on rituximab combined with cyclophosphamide, doxorubicin, vincristine, and prednisone (R-CHOP), most commonly in 21-day cycles. The exact therapeutic strategy depends on the individual patient's age and risk stratification scores and slightly varies among the guideline of the European Society for Medical Oncology (ESMO) published in 2015 and the more recent German and NCCN recommendations (11, 22, 31). In general, for younger (<60 years) low-risk patients, a reduced number of cycles while for older (>80 years) and/or frail patients, lower intensity treatment (such as R-miniCHOP or R-bendamustin) is recommended (11, 22, 31). At patients with elevated risk, rituximab, cyclophosphamide, doxorubicin, and prednisone is suggested to be amended with vindesine and bleomycin (R-ACVBP) or vincristine and etoposide (R-CHOEP or R-

EPOCH) or polatuzumab-vedotin (R-CHP-polatuzumab) (11, 22, 31). Involved site radiation therapy (ISRT) may be recommended in bulky disease (11, 22). The use of CNS prophylaxis is recommended in high-risk patients, in testicular lymphoma, in double- or triple-hit lymphoma, in leg type primary cutaneous lymphoma, in stage IE DLBCL of the breast, and in kidney or adrenal gland involvement, although the optimal therapeutic regime is debated (11, 22, 31).

Table 2. International Prognostic Index in DLBCL (11, 24)

International prognostic index (IPI)			Estimated 3-year overall survival (95% CI)
Risk factors	Age > 60 years		
	Serum LDH > upper limit of normal		
	Stage III–IV		
	ECOG PS 2–4		
	Extranodal sites >1		
Risk categories	Low	0–1	91% (89–94%)
	Low-intermediate	2	81% (73–86%)
	High-intermediate	3	65% (58–73%)
	High	4–5	59% (49–69%)

LDH: lactate-dehydrogenase; ECOG PS: Eastern Cooperative Oncology Group Performance Score (32); CI: confidence interval

Despite the improvements experienced with the introduction of rituximab, still about 20-40% of patients cannot be cured with frontline R-CHOP (30, 33). The therapy of early (< 12 months) relapsed disease or DLBCL refractory to frontline treatment is mainly based on novel, anti-CD-19 chimeric antigen receptor (CAR) T-cells therapy (11, 22, 31,

34). High-dose salvage chemotherapy with autologous haematopoietic stem-cell transplantation (ASCT) is preferred in disease relapse after 12 months (22, 34). Recently, more novel, promising options have become available for patients with relapsed/refractory disease not candidates for CAR-T-cells therapy or ASCT, as well as in second- or further-line settings, such as bispecific antibodies (blinatumomab, glofitamab, epcoritamab), the immunomodulatory drug lenalidomide, the cereblon E3 ligase modulator avadomide, novel monoclonal antibodies (loncastuximab tesirine), small-molecule inhibitors (ibrutinib, copanlisib, buparlisib, fostamatinib, venetoclax, temsirolimus, everolimus, bortezomib), as well as allogeneic haematopoietic stem cell transplantation (35-39).

1.2. PET/CT

1.2.1. Basics of PET imaging

1.2.1.1. Physical principals

The tracer-principle in nuclear medicine is based on the fact that substances labelled with a minimal (picomolar) amount of radioactive isotope (radiopharmaceuticals) do not pharmacologically affect metabolism but can be measured and visualised by appropriate means. PET is a medical imaging modality where substances labelled with positron emitting radioactive isotopes are traced and mapped. PET cameras are used to acquire three-dimensional (3D) data of the activity distribution in the human body, which is then plotted in different planes (usually transversal, coronal, and sagittal) or, by summing them up, even projection images.

Although atoms occurring in organic compounds, such as carbon, oxygen, and nitrogen have positron-emitter isotopes, their short half-lives (^{11}C: 20 min, ^{15}O: 2 min, ^{13}N: 10 min) reduce their implementation in clinical practice to label molecules for diagnostic purposes (40). Fluoride-18, on the other hand, with its physical half-life of 110 minutes is a more optimal radionuclide and with the synthesis of FDG it enabled a breakthrough in the molecular imaging of glucose metabolism (40). FDG enters cells through glucose transporters on the surface and undergoes the first phosphorylation step by hexokinase but the subsequent metabolite, FDG-6-phosphate is not a substrate of glucose-6-

phosphatase and it gets accumulated inside the cell (41). The signal of FDG-uptake is thus proportional to the rate of glucose metabolism.

1.2.1.2. Attenuation correction

In today's clinical routine, PET imaging is sequentially preceded by CT imaging utilizing a hybrid, PET/CT camera. The additional CT scan allows for correct spatial definition of PET-metabolic lesions and has value in characterising structures on its own. Furthermore, this CT image set can be used as a density map, and it allows for tissue attenuation correction (Figure 1).

1.2.1.3. Standardised Uptake Value

Implementing attenuation correction to PET images enables the quantisation of activity distribution measured by PET. The final, attenuation-corrected PET image is a set of voxels, virtual volumes with pre-defined dimensions. A specific activity-concentration can be attributed to each of these voxels and with the introduction of the Standardised Uptake Value (SUV), these activity-concentrations can be normalised by known variables in patient body weight and injected activity of the radiopharmaceutical as follows:

$$\text{SUV} = \frac{\text{Act}_{\text{VOI}}\,(\text{kBq}) \,/\, \text{V}_{\text{VOI}}(\text{mL})}{\text{Act}_{\text{administered}}\,(\text{MBq}) \,/\, \text{BW}\,(\text{kg})} \quad (23, 40)$$

(Act: activity; VOI: volume of interest; BW: body weight)

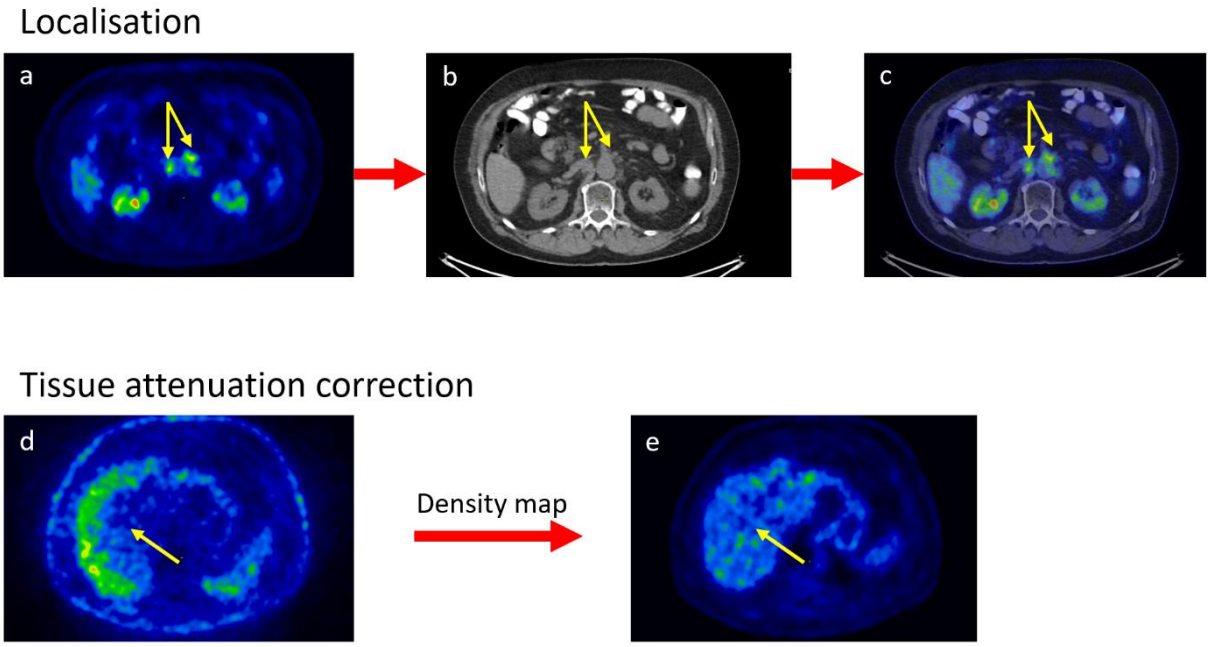

Figure 1. Utility of computed tomography (CT) in positron emission tomography (PET) diagnostics: localisation of small foci of uptake as lymph nodes (a-c) and tissue attenuation correction resulting in a more homogeneous tracer distribution in the liver, approximating the real distribution (d-e). PET/CT data are from the Semmelweis University, display is own work.

The resulting SUV values indicate the number of times the concentration of the tracer in the volume of interest (VOI) exceeds the value that would be measured in a hypothetical, completely uniform distribution throughout the body mass (23).

However, it is important to note that SUVs are exposed to several biologic (patient weight, blood glucose level, postinjection uptake time, respiratory motion) and technical (camera type, reconstruction parameters, calibration errors) factors that affect their values (42). This results in a challenge when comparing SUVs form PET scans acquired at different time points, and, especially, at different centres by different equipment. The impact of some of these affecting factors can be mitigated by a meticulous adherence to the imaging guidelines of the European Association of Nuclear Medicine (EANM) (23).

To harmonise the technological differences (mainly among various cameras and reconstructions), the EANM Research Ltd. (EARL) Harmonization Programme was introduced that utilises regular phantom measurements and consultancy based on central evaluation for each participating centre to reach a dedicated reconstruction method that produces SUVs mutually comparable among them (43). The EARL initiative recently proposed new standards to meet new demands set by point spread function (PSF) and time-of-flight (TOF) reconstructions (44).

Similarly to other medical imaging modalities, PET scans are present in the Digital Imaging and Communications in Medicine (DICOM) format in the daily routine.

1.2.1.4. Pitfalls in FDG-PET imaging

As the majority of malignant tumours present with increased glucose metabolism, FDG diagnostics can be utilised in their clinical management (23).

However, increased FDG accumulation is not exclusively tumour-specific as elevated glycolysis occurs in a number of physiological and pathological processes (45).

Consequently, in oncoheamatological use, FDG-PET/CT presents several normal variants and pitfalls where FDG-uptakes can be confused with malignant tissue, most importantly inflammatory processes as FDG accumulates in macrophages and other activated inflammatory cells, potentially leading to false-positive findings and decreased specificity (23, 40, 45, 46). Granulomatous diseases, mainly sarcoidosis and tuberculosis, can present similarly equivocal FDG-uptakes (47, 48).

Among further common factors reducing specificity, the following processes can present pitfalls: brown adipose tissue, skeletal muscle and mucosal activity, metformin-related colorectal uptake, peristaltic movements, physiological cycle-associated uptake in the endometrium and ovaries, diffuse reactive activity in the bone marrow or haematopoietic red bone marrow islands (23, 40, 45)

1.2.1.5. Novel reconstruction methods and impact on SUV

The conventional reconstruction method of raw PET data utilises ordered subsets expectation maximisation (OSEM) algorithms where, in general, the resolution recovery (RR; the difference between measured and true activity concentration in a VOI) is facilitated by the number of iterations, albeit at the cost of increasing noise levels which results in a compromise to reach optimal image quality in general practice (49). A novel reconstruction algorithm named Q.Clear was introduced to tackle this challenge by utilising a Bayesian penalised likelihood (BPL) method to reduce noise levels after each iteration cycle and to allow full image convergence (RR reaching 100%) (50). Q.Clear enabled better detection of small lesions and increase in lesion SUV_{max} values (51, 52). However, smaller (especially subcentimetric) lesions tend to be more affected than larger ones by the proportional increase of maximum SUV (SUV_{max}) values (52).

1.2.2. FDG-PET imaging in lymphomas

1.2.2.1. Applicability and utility of FDG-PET in lymphomas

Lymphomas differ in their glucose metabolic activity. Studies have shown that indolent lymphomas show lower FDG uptake than aggressive NHLs and Hodgkin's lymphoma (HL) (53, 54). For example, DLBCL and high-grade follicular lymphoma have on average three times higher SUV than low-grade follicular, lymphocytic-plasmocytic, marginal zone or small cell lymphoma, which are indolent lymphomas (55). The variable degree of FDG avidity can be explained mainly by different levels of proliferative activity, underlined by an analysis of PET/CT staging of 149 NHL patients where significant correlation was found between maximum SUV (SUV_{max}) and Ki-67 proliferation index (56).

A summary showed that 97-100% of both HLs and DLBCLs show FDG-avidity and as such, have negligible sensitivity limits in lesions above the spatial resolution of PET cameras, whereas, on the other end of the scale, only 40-60% of primary cutaneous T-cell lymphomas show considerable FDG-uptake (and neither of the investigated two cutaneous B-cell lymphomas were FDG-avid in the study) (54, 57).

1.2.2.2. Staging

Vast evidence has accumulated supporting the diagnostic superiority of PET – and especially PET/CT – in the staging of HLs and aggressive NHLs compared to conventional CT as more nodal and extranodal sites are confirmed by metabolic imaging, and as not only sensitivity but specificity is higher with PET/CT, correct evaluation of false-positive lesions on CT can also lead to downstaging (54, 58-60).

1.2.2.3. Treatment response assessment

PET imaging is able to distinguish between lymphoma and necrosis or fibrosis in residual masses and many studies showed that PET at the end of treatment is highly predictive of progression-free survival (PFS) and overall survival (OS) in aggressive lymphomas with or without residual masses detected with CT scan (61-63).

Currently, treatment response assessment is encouraged to be performed visually on PET scans using a 5-point-scale called Deauville-score (DS) which relates the most intense residual lymphomatous activity to references as the healthy liver parenchyma and the mediastinal blood-pool (Table 3 and Figure 2) (20, 54, 64). The standardised response evaluation set in the Lugano criteria considers residual metabolic disease at the end of treatment (EoT) with a DS of 4 or 5 as treatment failure, whereas scores 1-3 are attributed to complete metabolic response (CMR) as detailed in Table 4 (20, 54). Apart from the EoT setting, early response assessment or interim PET scans have been widely investigated and the utility of the DS is highlighted in the option to preset CMR as 1-2 or 1-3 depending on the aim of the study – for example, in trials that investigate therapy de-escalation based on PET-response, it may be more prudent to take a careful approach and consider DS3 as inadequate response to prevent undertreatment (20). On the other hand, in certain guidelines, DS4 at I-PET is considered as partial metabolic response and does not necessarily indicate treatment failure (34).

In general, current recommendations consider PET/CT as the first-choice imaging modality in HL and aggressive NHLs for staging and also for treatment response evaluation (20, 54). PET scans are not recommended in routine follow-up, mostly because

of the high rate of false-positive cases which is not clinically compensated for by its increased sensitivity (6).

More specific data on PET/CT in DLBCL are presented in the following sections.

Table 3. Deauville-score (DS), the most intense uptake in a site of initial disease (20, 54)

DS 1	No uptake
DS 2	Uptake ≤ mediastinum
DS 3	Uptake < mediastinum but ≤ liver
DS 4	Uptake moderately higher than liver
DS 5	Uptake markedly higher than liver and/or new lesions
DS X	New areas of uptake unlikely to be related to lymphoma

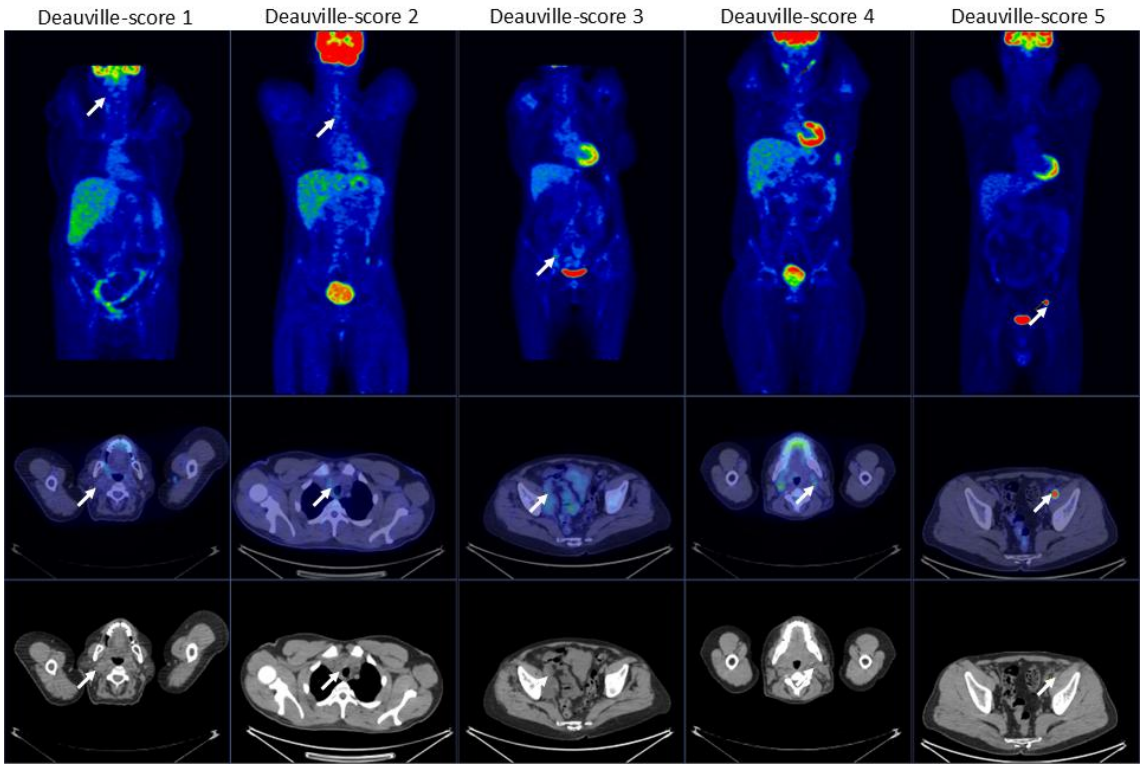

Figure 2. Demonstrative images of residual lymphoma lesion (arrows) uptake according to the Deauville-5-point-scale. Upper row: coronal FDG-PET images; Middle row: axial fused FDG-PET and CT images; Lower row: axial CT images. PET/CT data from the Semmelweis University, display is own work.

Table 4. Lugano criteria for the response assessment of HL and aggressive NHLs (20)

	Complete metabolic response	Partial metabolic response	No metabolic response	Progressive metabolic disease
Lymph nodes and extralymphatic sites	DS 1, 2, or 3 with or without a residual mass[1]	DS 4 or 5 with reduced uptake compared with baseline and residual mass(es) of any size	DS 4 or 5 with no significant change in FDG uptake from baseline	DS 4 or 5 with an increase in intensity of uptake from baseline and/or new FDG-avid foci consistent with lymphoma at interim or end-of-treatment assessment
New lesions	None	None	None	New FDG-avid foci consistent with lymphoma rather than another aetiology (e.g. infection, inflammation)[3]
Bone marrow	No evidence of FDG-avid disease in marrow	Residual uptake higher than uptake in normal marrow but reduced compared with baseline[2]	No change from baseline	New or recurrent FDG-avid foci

DS: Deauville-score

1 It is recognised that in Waldeyer's ring or extranodal sites with high physiologic uptake or with activation within spleen or marrow (e.g. with chemotherapy or myeloid colony-stimulating factors), uptake may be greater than normal mediastinum and/or liver. In this circumstance, complete metabolic response may be inferred if uptake at sites of initial involvement is no greater than surrounding normal tissue even if the tissue has high physiologic uptake.

2 Diffuse uptake compatible with reactive changes from chemotherapy is allowed. If there are persistent focal changes in the marrow in the context of a nodal response, consideration should be given to further evaluation with magnetic resonance imaging (MRI) or biopsy or an interval scan.

3 If uncertain regarding aetiology of new lesions, biopsy or interval scan may be considered.

1.3. PET in DLBCL

1.3.1. Baseline staging and prognostic PET biomarkers

1.3.1.1. Staging

Guidelines and recommendations are unanimous in prescribing PET/CT imaging for DLBCL staging (11, 20, 22, 31, 54). A prospective study investigating DLBCL patients found that PET/CT had a higher sensitivity than conventional CT and upward stage migration occurred in 15% of the cohort (58, 65).

An important aspect where PET/CT plays an additional role is bone marrow involvement. As has been shown in previous studies, PET/CT is more sensitive than bone marrow biopsy in DLBCL for the evaluation of bone marrow manifestation, although in 10-20% of the cases might miss low-volume diffuse involvement (20, 66-69). Therefore, in accordance with established guidelines and recommendations, a bone marrow biopsy is no longer mandatory when a PET/CT scan indicates advanced-stage disease through bone or marrow involvement. However, it remains a viable option with a negative PET result if its clinical relevance could potentially alter prognosis and treatment (11, 20, 22, 31, 58).

Apart from its inherent prognostic value through enabling accurate staging, baseline PET can provide more biomarkers that carry prognostic information.

1.3.1.2. SUV_{max}

SUV_{max} measured in the lymphomatous tissue(s) is a continuous semiquantitative value that is easily extractible from PET scans. Despite its wide availability, the prognostic value of baseline SUV_{max} is unclear in DLBCL. A recent systematic review found that only five out of the investigated twenty studies showed SUV_{max} having a significant impact on PFS and, interestingly, even these findings were inconclusive as two studies favoured higher SUV_{max} for longer PFS while three the lower values (70-75). The poor predictive significance of SUV_{max} may in part be attributed to its insufficient

representation of tumour load and its exclusive focus on the metabolic activity of the most aggressive cancer cells rather than the total tumour activity (71).

1.3.1.3. Metabolic Tumour Volume

Volumetric analysis of PET images enables to define VOIs encompassing lymphomatous tissue and the sum of these volumes yields the value referred to as metabolic tumour volume (MTV) or total metabolic tumour volume (TMTV) – within this thesis, the terminology of metabolic tumour volume is used. The delineation of the lesions can occur manually which is often user-dependent or to enhance reproducibility, with simple threshold-based methods or advanced lesion-growing algorithms (70, 76-80). Furthermore, in recent years fully automated MTV-segmentation methods have also been introduced (81, 82). So far, mainly threshold-based algorithms have been used in clinical studies and their diverse palette is presented in Table 5.

The prognostic value of MTV is more established. A systematic review that collated 19 studies found that 17 of them confirmed the impact of MTV on PFS (70). Moreover, a meta-analysis including 2729 lymphoma (mainly DLBCL) patients from 21 different studies showed that patients with a high baseline MTV had worse prognosis (83).

However, challenges hindered the implementation of MTV as a prognostic marker in routine practice. Firstly, the majority of published studies investigating baseline MTV were retrospective, heterogenous in methodology, and underpowered (70). Secondly, there is no consensus regarding which segmentation method should be utilised – and often the existing ones are vendor-dependent – which hinders the standardisation of MTV-based risk assessment through a definition of a robust cut-off point.

Most recently, an analysis of 1241 DLBCL patients from five previously published research studies found that a linear spline model was the best way to express the relationship between MTV (segmented uniformly as SUV≥4.0) and 3-year PFS, and furthermore, a new prediction model termed the International Metabolic Prognostic Index (IMPI) combining MTV, age, and stage was introduced that predicts relapse and survival better than the conventional IPI model (84).

To create a value encompassing SUV-based metabolic and MTV-based morphologic information, total lesion glycolysis (TLG) was introduced as the sum of the product of each lesion's metabolic volume and mean SUV (SUV_{mean}). Although several studies support the prognostic value of TLG, its superiority to MTV has not been proven, despite the more complex information it contains (70, 83, 85, 86).

Table 5. Different threshold-based MTV-segmentation algorithms

Lower threshold	**Isocontour**	**Other**
SUV≥2.5 or ≥4.0	40-41-42% of SUV_{max}	Majority vote[2]
≥1.0x or 1.5x SUV_{mean}(liver) + 2x or 3x SD(liver)	50% of SUV_{peak} [1]	Advanced (gradient-based) lesion growing
≥1.25x or ≥1.4x SUV_{max}(liver)		
≥SUV_{mean}(mediastinal blood pool)		

SUV: Standardised Uptake Value; SD: standard deviation

1 SUV_{peak} calculated as the mean SUV of a 12-mm-diameter sphere with highest local intensity; this algorithm also used background correction

2 consensus methods of previous algorithms

1.3.2. Interim PET/CT in DLBCL

1.3.2.1. The concept of interim PET

PET/CT in EoT settings has proved its robust ability to accurately evaluate treatment response and thus characterise future patient prognosis in DLBCL (61, 87-89). On this ground, EoT restaging PET/CT is incorporated in current DLBCL guidelines based on the Lugano recommendations utilising DS1-3 as adequate and DS4-5 as inadequate treatment response (11, 20, 22, 31, 54).

The results of EoT response assessment studies propelled research to investigate the crucial issue of utilising PET-based response assessment in an earlier setting – termed

interim PET (I-PET) – and guide further therapeutic methods to enable treatment change and escalation in non-responders and to avoid unnecessary toxicity through de-escalation in responders (61, 87-89).

1.3.2.2. Deauville-score

The most evidence have accumulated for the visual assessment with DS of interim PET scans for prediction of treatment response and prognosis of survival, pointing towards its superior performances compared to baseline IPI (54, 90-94). While the ESMO DLBCL guideline published in 2015 considered "mid-treatment imaging after three to four cycles "a possibility", it also pointed out that "changing treatment solely on the basis of interim PET/CT was discouraged", unless there is clear evidence of progression (11). Notwithstanding, the NCCN guideline published in December 2024 recommends performing interim PET/CT in every case after two, three or four cycles of therapy where DS1-3 is classified as complete response (CR) and further management is dependent on whether the patient had achieved CR (34).

However, despite being robust and easy to implement in clinical routine, the accuracy of DS faces challenges.

In general, there is little consensus and up until 2021, no comprehensive publication was published about the optimal timing of interim PET – this latter analysis reported that interim PET predicted good response equally after two (I-PET2) and four cycles (I-PET4) of R-CHOP and recommended I-PET2 for de-escalation trials (this study also suggested I-PET4 for randomised trials investigating new therapeutics with ΔSUV_{max}-based evaluation, a method detailed in a later section) (95). Regarding exact timing between treatment cycles, it is suggested for interim PET to wait at least 10 days after chemotherapy to prevent the "stunning" effect of therapy on tumour cells and 13-14 days following the last treatment cycle to avoid nonspecific FDG uptake caused by inflammation resulting from chemotherapy and rituximab (96-98).

A marked limitation is that DS is an ordinal and not a continuous scale and though its experience-backed but arbitrary cut-off between DS3 and DS4 has good to excellent negative predictive value (NPV) generally exceeding 80%, its positive predictive value

(PPV) is markedly lower at 20-74% in estimating progression- or event-free survival, arising mainly from the fact that several patients with an interim DS of 4 never experience relapse (91, 92, 99-106).

This observation has been exacerbated by the recent introduction of novel PET-reconstruction algorithms that tend to yield a higher SUV and thus a more intense visual appearance in DS evaluation than images acquired with conventional algorithms that were used for the validation of DS-based stratification, leading to an increased number of misclassified DS4 patients (107-109).

1.3.2.3. ΔSUV_{max}

Given the limitations of the DS method, continuous-scaled prognostic values have been investigated, most prominently the ΔSUV_{max} method.

ΔSUV_{max} is the proportional change in maximum standardised uptake value of the most intense residual lesion between interim and baseline PET as in the following formula:

$$\Delta SUVmax = \frac{SUV_{max}(interim) - SUV_{max}(baseline)}{SUV_{max}(baseline)}$$

SUV_{max}: maximum standardised uptake value

Its most commonly used cut-off value is 66% decrease in SUV_{max} at I-PET2 or I-PET3 while the 70% value is frequently used at I-PET4 (102, 106, 110-112). It has also been shown that ΔSUV_{max} evaluation outperforms the DS method in predicting treatment response in DLBCL patients, especially at I-PET4 (95, 112-114).

1.3.2.4. Novel continuous interim parameters

Researched with less intensity than ΔSUV_{max}, "Deauville-like" continuous parameters have also been introduced in quantitative PET (qPET) and ratio PET (rPET); their formula is as follows:

$$qPET = \frac{SUV_{peak}(lesion)}{SUV_{mean}(liver)} \qquad rPET = \frac{SUV_{max}(lesion)}{SUV_{max}(liver)}$$

SUV_{peak}(lesion): average over the maximum SUV voxel and the three hottest adjacent ones

SUV_{mean}(liver): average uptake in a 30 mL cuboid VOI (length:width:height = 2:2:1) positioned in the right liver lobe

First used in the prospective EuroNet-PHL-C1 trial (EudraCT 2006-000995-33), qPET gained recognition in paediatric HL which study found that classification by qPET≥2.0 or DS5 had better predictive value than that with qPET≥1.3 or DS4-5 (115-117). The suitability of qPET was later validated in adult HL and DLBCL (118, 119).

The parameter rPET has only been investigated in smaller, retrospective studies in HL and DLBCL, with their main findings detailed in Table 6 (100, 120, 121).

Table 6. Studies utilizing rPET in prognostic evaluation of DLBCL

First author, year (reference number)	**Number of patients included**	**Lymphoma type**	**Interim PET**	**Endpoint**	**Optimal cut-off point**
Annunziata, 2016 (120)	68	HL	After 2 cycles	2-year PFS	1.14
Fan, 2017 (100)	119	DLBCL	After 2 cycles	2-year PFS and OS	1.6 for PFS 1.7 for OS
Toledano, 2019 (121)	181	DLBCL	After 4 cycles	5-year PFS and OS	1.4 for both PFS and OS

rPET: ratio-PET; HL: Hodgkin's lymphoma; DLBCL: diffuse large B-cell lymphoma; PFS: progression-free survival; OS: overall survival

1.3.2.5. Challenges of SUV-based methods

Despite the fact that SUV is readily available from routine PET scans, the implementability of response assessment methods based on this semiquantitative value face some problems.

The comparison of SUVs of PET scans from different centres (e.g. at multicentre trials) is compromised due to variations in image acquisition settings, such as the scanner and the reconstruction algorithm utilised (including scatter and attenuation correction) (122). By normalising the SUV of the tumour to a reference region – most commonly the liver – in the same PET scan, this issue is significantly mitigated because, in most cases, both regions are affected by the technological differences and will, to some extent, counteract each other (122).

Hence, it is advisable to employ tumour-to-reference organ SUV ratios instead of straight SUV values when comparing outcomes obtained from various scanners (122).

Furthermore, the phenomenon of partial volume effect might lead to a significant underestimation of the actual activity concentration within a lesion, especially as post-treatment lymphoma residuals are frequently small (122-124). The reconstruction algorithm can have a significant impact on this. Similarly to BPL methods, the utilisation of PSF and TOF reconstruction enhances the detectability and raises the SUVs of tiny lesions, while leaving the SUVs of reference organs such as the liver unaltered (122, 125). Regarding the evaluation, this effect has the potential to undermine both the visual DS and the semiquantitative tumour-to-reference organ SUV ratios (122, 125-127).

Biological factors also have an impact on the comparability of SUVs, most importantly uptake time in which case tumour uptake keeps increasing for more than ninety minutes after injection whereas activity concentration in liver and mediastinal reference regions plateau (122).

In conclusion, rigorous attention should be paid for the major influencing factors of SUVs in order to design novel response evaluation criteria that reach the required robustness and reliability for widespread clinical implementation.

1.4. Radiomics

1.4.1. Background

Radiomics or texture analysis aims to extract quantitative, and ideally reproducible, information from diagnostic images, including complex patterns that are difficult to recognise or quantify by the human eye (128-130).

The first implementation of textural analysis in medical imaging dates back to 1972 when Sutton *et al.* investigated the automated classification of X-ray images in pulmonary diseases (131). It was first the spread of digital images then the exponential improvements in computational capacity that led to the prominent acceleration in medical imaging radiomics research (132).

Radiomics can be utilised to capture the characteristics of tissues and lesions, including their form and heterogeneity and the oncologic relevance of the latter is further underlined by molecular genetic research showing that the level of tumour heterogeneity is a prognostic factor and poses a challenge to cancer management (104, 128, 133).

1.4.2. Steps to perform radiomics analyses

1.4.2.1. Segmentation

There is a lack of agreement on the appropriate method for segmenting the structure of interest prior to conducting radiomic analysis (128, 134). Numerous studies have shown that radiomic features are highly influenced by the segmentation method employed. In order to ensure reproducibility, it is more advisable to utilise an automated or semi-automated approach than human segmentation and to minimise the variability in radiomic feature values caused by differences in the definition of VOIs, it is recommended to employ a consistent approach for all patients within the cohort (128, 134).

1.4.2.2. Spatial resampling and intensity discretisation

Spatial resampling is used to achieve isotropic voxels (cubes with the same length of edges) of the same size and intensity discretization is a necessary process for calculating certain radiomic properties that involves grouping close grey levels together to minimise the influence of noise (128, 134).

1.4.2.3. Feature extraction

The radiomic features are calculated in the segmented region after spatial resampling and intensity discretization, except for "native" features that do not require any binning for calculation (e.g. SUV_{max}, SUV_{mean}, SUV_{peak}, MTV, and TLG) and the objective is to precisely measure the quantitative properties of the distribution of voxel values, the form of the VOI, and the spatial correlation between voxel values within the VOI (128, 134, 135). Types of these features are detailed in later sections.

1.4.2.4. Feature harmonisation, selection, and reduction

Harmonisation is a mathematical technique used to eliminate the batch effect, which refers to the centre-dependent effects caused by differences in acquisition parameters, on radiomic characteristics. This technique is applied after image capture, reconstruction, and analysis, directly to numeric radiomic feature values, rather than to pictures. After the completion of radiomic image analysis, it is necessary to identify the pertinent aspects that will be utilised in the statistical model to address the clinical issue, such as distinguishing between benign and malignant lesions. While it is theoretically possible to employ the hundreds of radiomic feature candidates retrieved as input for the prediction model, doing so would result in an exponential increase in the number of required model parameters. Hence, a substantial quantity of potential features must be eliminated or modified through a procedure termed as dimensionality reduction (128, 134, 135).

1.4.2.5. Model building

Once the radiomic traits have been chosen, they are employed to predict target variables, such as the presence or absence of a disease or tumour type, or response to therapy or overall/progression-free survival.

Machine learning models acquire knowledge about the correlation between inputs with multiple dimensions, specifically radiomic characteristics, and target variables by analysing a set of training samples. An important ability is the use of sets of predictors or features, known as multivariate patterns, rather than relying on univariate or mass-univariate regression.

Utilising cross-validation systems, where training and test sets are systematically rotated within the available data, might mitigate the constraints imposed by small dataset sizes. However, it is crucial to exercise caution while employing such schemes.

Aside from the above, conventional "handcrafted" methodology, "deep-radiomics" utilizing convolutional neural networks (CNNs) have also been implemented where the radiomic features are acquired by the CNN itself based on the input images and the task at hand (128, 134).

1.4.3. Types of radiomic features

Texture features are categorised into first-, second-, and higher orders by the number of voxels involved in their texture matrix design (128, 134, 135).

First-order textural features describe global characters of a tumour on PET images and are calculated from the intensity frequency histogram which represents the frequency distribution of one-voxel intensity in a segmented lesion (134, 135). First-order metrics include conventional PET parameters such as SUV (max, mean, peak), MTV and TLG, as well as more complex variables in the skewness and kurtosis representing the shape of the histogram, and the first-order energy and entropy (128, 134, 135).

The second-order parameters can be obtained from the analysis of the grey-level cooccurrence matrix (GLCM) which defines space by voxel pairs and examines the frequency with which the pairs take up the different grey level values (128, 135, 136).

When examining voxel pairs, their orientation is non-negligible, thus when characterising a volume, each direction of the space needs to be mapped by a cooccurrence matrix (135, 136). The radiomic parameters that can be extracted from the GLCM are second-order entropy and energy, heterogeneity, homogeneity, contrast (intensity differences of voxel pairs), and dissimilarity (128, 135).

Higher-order textural features are calculated from different types of texture matrices computed based on interrelationships of three or more voxels (135, 137). Neighbourhood grey-tone difference matrices (NGTDMs) compute for differences between each voxel and neighbouring voxels within a certain distance (features include coarseness, contrast, and busyness that represent local texture within a segmented lesion), Grey-level run-length matrices (GLRLMs) measure for runs of voxels with same grey-level along a given direction while Grey-level size zone matrices (GLSZMs) consider the size of continued voxels with same grey-level (135, 138, 139).

1.4.4. Radiomics of PET scans in DLBCL

To date, peer-reviewed publications involving radiomic analysis of PET scans in DLBCL patients have been relatively scarce, mainly retrospective and single-centre, also heterogeneous in endpoint and methodology (140). Table 7 encompasses the main attributes of recent publications (74, 141-154).

Table 7. Summary of publications of radiomics in DLBCL

First author, year	Number of patients included	Lymphoma type	Segmentation method	Endpoint	Statistical method	Discriminating radiomic parameters
Parvez, 2018 (141)	82	NHL, mainly DLBCL (93.9%)	SUV≥3.0	DFS, OS	Cox regression	DFS: LZE, LZLGE, GLNU OS: MTV, TLG, kurtosis
Aide, 2018 (142)	82	DLBCL	Skeletal, manually	PFS, OS	Cox regression	PFS: skewness, kurtosis OS: skewness, kurtosis, entropy, energy, SZHGE
Zhou, 2019 (143)	35	PG-DLBCL	40% SUV_{max}	PFS, OS	Cox regression	PFS: MTV, coarseness, GLRLM, RLNU OS: MTV, coarseness, GLRLM, kurtosis
Aide, 2020 (144)	132	DLBCL	SUV≥2.2 (SUV>liver for MTV)	EFS	Cox regression	MTV, LZHGE
Sun, 2020 (145)	30	PGIL-DLBCL	41% SUV_{max}	Interim response**	Logistic regression	SUV_{max}, volume, entropy, energy
Lue, 2020 (146)	83	DLBCL	SUV≥2.5	PFS, OS	LASSO	PFS, OS: RLNU
Cottereau, 2020 (147)	95	DLBCL	41% SUV_{max}	PFS, OS	Cox regression	PFS, OS: MTV, $Dmax_{patient}$
Coskun, 2021 (148)	45	DLBCL	40% SUV_{max}	Response to treatment**	Logistic regression	SUV_{max}, GLCM dissimilarity
Ceriani, 2022 (74)	107	DLBCL	SUV≥4.0	PFS, CSS, OS	LASSO	RS index
Ritter, 2022 (149)	85	DLBCL	SUV>liver	EFS	Mixed ensemble learning	MTV, TLG, $Dmax_{lesion}$, busyness, coarseness

Table 7. Summary of publications of radiomics in DLBCL (continued)

First author, year	Number of patients included	Lymphoma type	Segmentation method	Endpoint	Statis-tical method	Discriminating radiomic parameters
Eertink, 2022 (150)	317	DLBCL	SUV≥4.0	TTP	Logistic regres-sion	MTV, SUV_{peak}, $Dmax_{patient}$
Cui, 2023 (151)	271	DLBCL	SUV≥4.0	TTP	Cox regres-sion	Cluster prominence, IMC1, LAHGLE $Dmax_{lesion}$
Jing, 2023 (152)	201	DLBCL	SUV≥4.0	PFS, OS	LASSO	PFS: $Dmax_{lesion}$, LRLGLE, SZNUN OS: 10 parameters
Li, 2023 (153)	129	DLBCL	41% SUV_{max}	PFS	Cox regres-sion	Rad-score (including elongation and coarseness)
Eertink, 2023 (154)	1195	DLBCL	SUV≥4.0	TTP, PFS	Logistic regres-sion	MTV, SUV_{peak}, $Dmax_{patient}$

*(both SUV≥3.0 and SUV≥6.0 for MTV) **(DS1-3)

NHL: non-Hodgkin lymphoma; DLBCL: diffuse large B-cell lymphoma; PG: primary gastric; PGIL: primary gastrointestinal; SUV: standardised uptake value; MTV: metabolic tumour volume; DFS: disease-free survival; OS: overall survival, PFS: progression-free survival; EFS: event-free survival; CSS: cause-specific survival; TTP: time to progression; LASSO: least absolute shrinkage and selection operator; LZE: long-zone emphasis; LZLGE: long-zone low grey-level emphasis; GLNU: grey-level nonuniformity; TLG: total lesion glycolysis; SHZGE: short-zone high grey-level emphasis; GLRLM: grey-level run-length matrix; RLNU: run length non-uniformity; LZHGE: long-zone high grey-level emphasis; $Dmax_{patient}$: the maximal distance between the largest lesion and any other lesion; GLCM: grey-level cooccurrence matrix; RS: radiomics score; $Dmax_{lesion}$: maximum lesion diameter; IMC1: informational measure of correlation; LAHGLE: large area high grey-level emphasis; DS: Deauville-score

2. OBJECTIVES

Although PET/CT is an important imaging method in the management of DLBCL patients and has substantial potential in prognostic estimations, all the different PET-based biomarkers have their limitations which on occasions hinder their widespread utilisation in clinical practice. A main hindrance is the relatively low PPV of several biomarkers which limits their use in PET-based treatment escalation.

In general, my research aimed to explore the options of current PET biomarkers in DLBCL prognostic evaluation with a particular focus on novel additions to existing methods that could be easily implemented in routine practice and have the potential of enhancing current prognostic efficacy.

With the above conception, first, a reanalysis of a multicentre trial is presented that investigated baseline and interim PET biomarkers in DLBCL prognosis evaluation. As several different methods exist and, at the time of the research, no consensus was present regarding the optimal MTV segmentation, a specific emphasis was put on evaluating data acquired by three different methods. Also, as an incentive of standardisation, volumetric values were normalised to body weight. Furthermore, as a potential upgrade to the ordinal-scale DS, continuous-scale semiquantitative parameters were investigated on interim PET.

Secondly, data of a cohort from a single centre was used to investigate possible PET biomarkers to improve the prognostic ability of baseline MTV. With that aim, a novel value, MTVrate was introduced as the quotient of the largest lesion's volume and total body MTV and radiomics were also incorporated in the analysis.

2.1. Prognostic parameters on baseline and interim FDG-PET/CT in DLBCL patients

1. How is the prognostic accuracy of baseline volumetric PET parameters influenced by different segmentation methods and is there an additive value in standardising them to body weight?
2. What is the prognostic efficacy of different baseline and interim PET parameters in a prospective, multicentre study?

2.2. Volumetric and textural analysis of PET/CT in patients with DLBCL, introducing the importance of novel MTVrate feature

3. What is the prognostic value of baseline clinical, volumetric, and radiomics-based textural parameters individually and in a combined analysis with a machine learning algorithm in a retrospective, single-centre study?
4. Is there an additive value of the newly introduced MTVrate parameter?

3. METHODS

3.1. Prognostic parameters on baseline and interim FDG-PET/CT in DLBCL patients

3.1.1. Patient cohort

Data and images of a multicentre clinical trial initiated and sponsored by the International Atomic Energy Agency (IAEA) were re-evaluated in the current analysis. In the original IAEA study, titled "Application of FDG-PET and Molecular Gene Profiling for Risk Stratification of Diffuse Large B-cell Non-Hodgkin's Lymphoma in Different Ethnic Populations", DLBCL NOS patients were recruited in 10 centres across the world (São Paulo, Brazil; Santiago, Chile; Budapest and Debrecen, Hungary; Mumbai, India; Bologna, Italy; Seoul, South Korea; Manila, Republic of the Philippines; Bangkok, Thailand; and Ankara, Türkiye) (104). In order to reach a more homogeneous cohort, several exclusion criteria were applied to the original trial, detailed in Table 8.

Table 8. Exclusion criteria from the IAEA trial

Patient age < 16 years
Primary central nervous system or bone lymphoma
Cancer within the preceding 5 years
Steroid therapy before the staging scan
No FDG–avid disease on baseline PET
Treatment other than R-CHOP
Studies performed on a stand-alone PET scanner
Studies performed on different PET/CT scanners in baseline and interim setting
Missing or compromised imaging data
Event-free follow-up lasting less than 24 months

FDG: 2-[^{18}F]fluoro-2-deoxy-D-glucose; PET: positron emission tomography; CT: computed tomography; R-CHOP: rituximab combined with cyclophosphamide, doxorubicin, vincristine, and prednisolone

The clinical stage was assessed using the baseline PET/CT scans, according to the Lugano modification of the Ann Arbor criteria (20). Additionally, the R-IPI score was calculated for each patient (27).

3.1.2. PET biomarkers

PET/CT image evaluation was performed with Mediso InterView Fusion software (Mediso Medical Imaging Systems, Budapest, Hungary). Lymphoma lesions were segmented on baseline PET/CT scans with three different methods: 1) SUV>4.0 (glob4); 2) 41% isocontour VOI around the local maximum point (41pc); 3) a vendor-specific gradient-based lesion growing algorithm (grad). The sum of all lymphoma lesions' volume on PET images yielded MTV. TLG was calculated as the sum of the product of each lesion's metabolic volume and SUV_{mean}. Both MTV and TLG values were normalised for patient body weight, thus introducing bwaMTV and bwaTLG values.

Visual and semiquantitative analyses were performed of the interim PET/CT scans, the former according to the Deauville-five-point scale and the Lugano criteria (Table 3 and 4, Figure 2) (20, 54).

Semiquantitative interim parameters were based on SUV-measurements in the most active lymphoma lesions and in a 3 cm diameter spheric VOI placed in the healthy/unaffected part of the right liver lobe. The resulting parameters encompassed ΔSUV_{max}, rPET, and modified qPET (mqPET) values.

ΔSUV_{max} was defined as the proportional change in the SUV_{max} of the most active lymphoma lesion in percents between interim and baseline PET/CT scans. It is important to note that this calculation indicates the decrease with a numeric constant (minus sign) in front of the ΔSUV_{max} value and lower values suggest better treatment response.

The rPET value, as described before, is the proportion of the SUV_{max} in the hottest lesion and the SUV_{max} in the reference VOI in the liver parenchyma. The original qPET value was first introduced in paediatric Hodgkin's lymphoma and defined SUV_{peak} – in the numerator of the quotient – as the mean SUV of the hottest 4 adjacent voxels in the lesion (115). In the current analysis including only adult DLBCL patients SUV_{peak} was defined by the more common – and thus, more readily available among different softwares –

method of averaging SUVs in the hottest virtual volume of 1 cm^3 (1 mL). Consequently, the 1 cm^3 SUV_{peak} of the most intense residual lymphoma lesion divided by the SUV_{mean} of the liver reference VOI resulted in the parameter termed modified qPET (mqPET) in the present study.

3.1.3. Statistical analysis

Pearson-correlation tests were used to compare volumetric parameters (MTV and TLG) by different segmentations. 24-month PFS served as the endpoint for the prognosis analyses. Optimal cut-off points were defined by receiver operating characteristics (ROC) analyses for MTV, TLG, bwaMTV, and bwaTLG values acquired by the three different segmentation methods as well as for interim semiquantitative parameters in ΔSUV_{max}, mqPET, and rPET. Based on the ROC-based optimal cut-off points, patients were divided into high- and low-risk groups according to the different PET-biomarkers and the PFS of these groups were investigated with log-rank analyses, as well as univariate and multivariate Cox-regression analyses. P-values less than 0.05 were considered statistically significant.

3.2. Volumetric and textural analysis of PET/CT in patients with DLBCL, introducing the importance of novel MTVrate feature

3.2.1. Patient cohort

Baseline PET/CT scans of consecutive DLBCL NOS patients acquired at the Department of Nuclear Medicine of Semmelweis University's Medical Imaging Centre between 2017 and 2019 were included in the study. All patients in the cohort received rituximab-based immunochemotherapy – mostly R-CHOP – with a curative intent and had complete medical data to determine IPI, phenotype of DLBCL, and follow-up events or census.

At staging PET/CT, patients received 2.5-3.0 MBq/body weight kilogram FDG intravenously after a fasting period of more than six hours. 60 minutes after the injection of the radiopharmaceutical, a native CT scan and 3D PET-emission imaging were

acquired with a hybrid PET/CT system (GE Discovery IQ5, GE Healthcare). PET data were reconstructed using a novel BPL method-based algorithm (Q.Clear) and in some cases, with a conventional OSEM algorithm (with 6 iterations and 6 subsets).

3.2.2. PET biomarkers

Baseline PET images were evaluated by Mediso InterView Fusion software (Mediso Medical Imaging Systems, Budapest, Hungary) and lymphoma lesions were delineated using a fixed SUV-based semi-automatic algorithm (SUV > 4.0 values) and were corrected manually when needed, to establish VOIs (Figure 3). MTV was calculated as the sum of all lymphoma lesions' volume on PET images, and TLG was determined as the sum of the product of each lesion's metabolic volume and SUV_{mean}.

MTVrate was introduced as the quotient of the largest lesion's volume and total body MTV.

The VOI of the largest lymphoma lesion was used to extract first-, second-, and higher-order textural features, 44 in total. Patients with volume of the largest lymphoma lesion under 30 cm^3 were excluded to avoid dependence on volume when calculating second-order entropy [26].

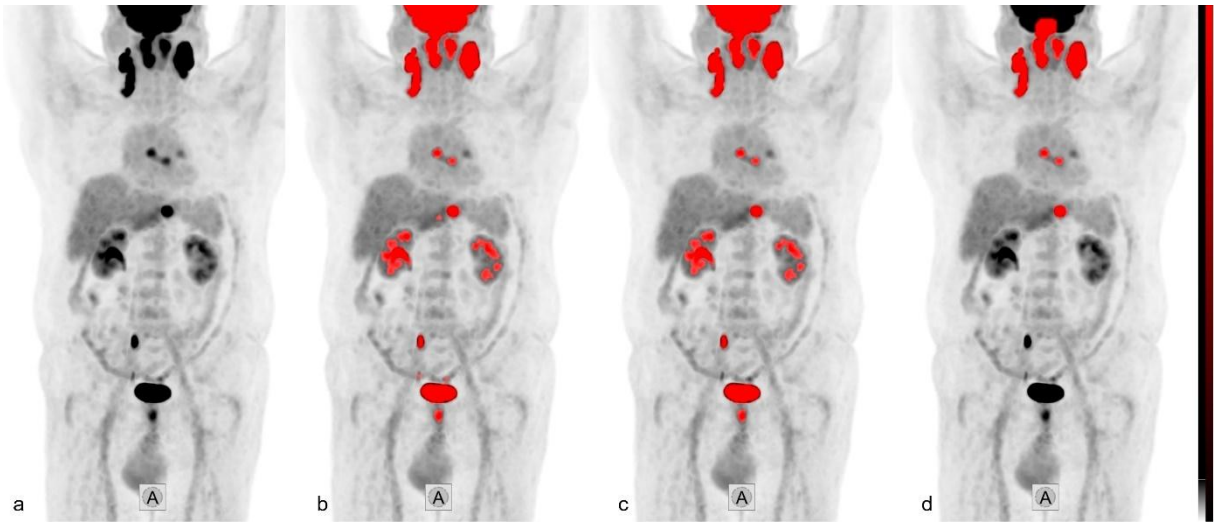

Figure 3. Segmentation algorithm of the lymphoma lesions on three-dimensional PET maximum intensity projection images; tumour delineations are indicated in red. a) starting

point; b) automatic segmentation of voxels with SUV > 4.0; c) elimination of volumes less than 1 cm^3; d) elimination of non-lymphomatous volumes. PET data are from the Semmelweis University, display is own work.

SUV: standardised uptake value

3.2.3. Statistical analysis

ROC analyses were performed to assess the prognostic performance of clinical and PET-based (volumetric and textural) values and to define optimal cut-off points. These cut-off points were used to determine low- and high-risk groups for each biomarker and the PFS of these groups was evaluated by log-rank analysis.

Where both OSEM and Q.Clear PET-reconstructions were available, lesion-segmentation was performed individually on both image sets and intraclass correlation coefficients (ICCs) were calculated.

Finally, a machine learning algorithm was used to build a prognostic model from the available clinical, volumetric, and textural data based on logistic regression. To avoid overfitting, we utilised elastic net regularization, the sum of L1 (Lasso) and L2 (Ridge) regularization functions. After preprocessing, repeated cross-validation was used to train the model in three cycles, randomly splitting the patient population 70% : 30% into training and test sets (with reassigning after the first and second round). The model cleared the redundant parameters and gave the remaining ones relative importance. At the end, ROC-analysis was performed with the model to determine its prognostic value.

4. RESULTS

4.1. Prognostic parameters on baseline and interim FDG-PET/CT in DLBCL patients

4.1.1. Patient characteristics

After the exclusions, 107 patients were included in the present study (median age: 56; range: 16-83 years) with 53 women and 54 men among them. The majority of patients were from Hungary (57) and Chile (36), while 8, 4, and 2 of them were from Thailand, the Republic of the Philippines, and Italy, respectively. A third of the patients had poor R-IPI score and 58% of them presented with advanced stage disease (Table 9).

Progression-free survival in the whole cohort was 75%. Interestingly, neither univariate Cox-regression analysis, nor log-rank analysis showed a significant difference between survival and risk of progression of early and advanced stage patients (PFS: 82% vs. 69%).

4.1.2. Volumetric parameters

Good to excellent correlation was observed among MTV and TLG values segmented by glob4, 41pc and grad methods as demonstrated in Table 10. ROC analyses yielded markedly different optimal cut-off points for MTV, TLG, bwaMTV, and bwaTLG with the three different segmentation methods, but areas under the curve (AUCs) did not show a significant difference between standard and body weight-adjusted volumetric parameters (i.e. MTV vs. bwaMTV and TLG vs. bwaTLG) with the corresponding segmentation methods. Greater variability in sensitivity, specificity, positive and negative predictive values, and diagnostic accuracy was seen, mostly among the same volumetric parameters acquired by different segmentation methods, rather than between traditional and body weight-adjusted MTV or TLG. Univariate Cox-regression analyses showed significantly different risk of progression between groups divided by the ROC-based optimal cut-off value in all cases except for bwaTLGglob4. Detailed values are presented in Table 11 for MTV and Table 12 for TLG.

Table 9. Patient characteristics and clinical data

Characteristic		**n= 107 (100%)**
Sex	Male	54
	Female	53
Age	Range	16-83
	Median	56
	>60 years	44 (41%)
ECOG PS	0-1	83 (78%)
	2-4	24 (22%)
Stage	I	16 (15%)
	II	29 (27%)
	III	19 (18%)
	IV	43 (40%)
R-IPI	Very good (score: 0)	24 (22%)
	Good (score: 1-2)	48 (45%)
	Poor (score: 3-5)	35 (33%)
Timing of interim PET/CT	After 2 cycles of R-CHOP	90 (84%)
	After 3 cycles of R-CHOP	17 (16%)

ECOG PS: Eastern Cooperative Oncology Group Performance Score (32); R-IPI: Revised International Prognostic Index; R-CHOP: rituximab combined with cyclophosphamide, doxorubicin, vincristine, and prednisolone

Table 10. Pearson-correlation coefficients between volumetric parameters by different segmentation methods

MTV	*41pc*	*grad*		**TLG**	*41pc*	*grad*
glob4	0.872	0.849		*glob4*	0.981	0.984
41pc		0.962		*41pc*		0.993

MTV: metabolic tumour volume; TLG: total lesion glycolysis; bwa: body weight-adjusted; glob4: >SUV4 method; 41pc: 41% isocontour VOI method; grad: method using a gradient-based lesion growing algorithm

Preserving the risk-labelling according to the ROC-analysis optimum in the whole cohort, the predictive values were investigated of the above baseline PET-volumetric parameters according to clinical stage. NPV ranged between 87.2-96.3% (lowest for bwaMTVgrad and highest for bwaTLG41pc) for early stage and between 80.0-90.5% (lowest for bwaTLGglob4 and highest for MTV41pc) for advanced stage, respectively. PPV ranged between 16.7-37.5% (lowest for bwaTLGgrad and highest for MTVgrad) for early stage and between 32.0-44.8% (lowest for TLGglob4 and highest for bwaTLGgrad) for advanced stage, respectively.

A similar analysis of the baseline PET-volumetric parameters was performed according to R-IPI scores. NPV ranged between 83.1-94.7% (lowest for bwaTLGgrad and highest for bwaTLG41pc) for patients with R-IPI scores 0-2 (n=72) and between 71.4-92.3% (lowest for bwaTLGglob4 and highest for both MTVgrad and bwaTLGgrad) for patients with R-IPI scores 3-5 (n=35), respectively. PPV ranged between 23.1-38.5% (lowest for bwaTLGgrad and highest for bwaMTVgrad for patients with R-IPI scores 0-2 (n=72) and between 34.4-50.0% (lowest for TLGglob4 and highest for both MTVgrad and bwaTLGgrad) for patients with R-IPI scores 3-5 (n=35), respectively.

4.1.3. Interim parameters

Regarding interim PET parameters, optimal cut-off points on ROC analyses were -71.22%, 1.32, and 1.54 for ΔSUV_{max}, mqPET, and rPET, respectively and univariate Cox-regression analyses showed significantly different risk of progression between groups divided by these values. These data, accompanied by AUCs, sensitivity, specificity, positive and negative predictive values, and diagnostic accuracy of interim parameters are detailed in Table 13.

Table 11. Descriptive statistics, cut-off values, areas-under-the-curve (AUCs), diagnostic performance and univariate Cox-regression analyses of MTV and bwaMTV acquired by different segmentation methods

	MTV			bwaMTV		
	glob4	41pc	grad	glob4	41pc	grad
Minimum	1	2	1	0.02	0.03	0.02
Maximum	3268	4470	3841	38.9	53.2	45.5
Median	170	269	200	2.5	3.5	2.7
Average	426	590	497	6.2	8.4	7.0
SD	571	816	696	8.3	11.3	9.2
Cut-off	*122.5*	*257.5*	*334.9*	*2.55*	*2.68*	*7.84*
AUC	0.63	0.65	0.66	0.65	0.67	0.68
Sensitivity	77.8%	74.1%	63%	66.7%	77.8%	55.6%
Specificity	47.5%	56.3%	70%	56.3%	57%	76.2%
PPV	33.3%	36.4%	41.4%	34.0%	36.2%	44.1%
NPV	86.3%	86.5%	84.8%	83.3%	89.1%	83.6%
Accuracy	55.1%	60.7%	68.2%	58.9%	61.9%	71%
HR* (95% CI)	2.7 (1.1-6.8)	3.1 (1.3-7.4)	3.3 (1.5-7.2)	2.4 (1.1-5.4)	3.4 (1.4-8.4)	3.4 (1.6-7.2)
p*	0.03	0.01	0.003	0.031	0.008	0.002

*: univariate Cox-regression analysis

MTV: metabolic tumour volume; bwa: body weight-adjusted; glob4: >SUV4 method; 41pc: 41% isocontour VOI method; grad: method using a gradient-based lesion growing algorithm; SD: standard deviation; PPV: positive predictive value; NPV: negative predictive value; HR: Hazard ratio; CI: confidence interval

Table 12. Descriptive statistics, cut-off values, areas-under-the-curve (AUCs), diagnostic performance and univariate Cox-regression analyses of TLG and bwaTLG acquired by different segmentation methods

	TLG			bwaTLG		
	glob4	41pc	grad	glob4	41pc	grad
Minimum	6	10	6	0.08	0.14	0.09
Maximum	32943	33146	30975	388.1	378.5	350.0
Median	1337	1656	1548	18.8	25.4	20.2
Average	3943	4434	4108	57.0	63.8	58.9
SD	5743	6095	5670	81.5	86.3	79.7
Cut-off	*714.7*	*1207*	*2112*	*15.5*	*13.2*	*53.3*
AUC	0.62	0.64	0.65	0.63	0.65	0.65
Sensitivity	81.4%	77.8%	62.9%	70.4%	77.8%	51.9%
Specificity	41.3%	51.3%	62.5%	51.3%	48.8%	73.8%
PPV	31.9%	35%	36.2%	32.8%	33.9%	40.0%
NPV	86.8%	87.2%	83.3%	83.7%	86.7%	81.9%
Accuracy	51.4%	57.9%	62.6%	56.1%	56.1%	68.2%
HR (95% CI)*	2.7 (1-1.7)	3.1 (1.3-7.8)	2.5 (1.2-5.6)	2.2 (0.98-5.1)	3.2 (1.2-8.4)	2.7 (1.3-5.7)
p*	0.047	0.014	0.019	0.057	0.02	0.01

*: univariate Cox-regression analysis

TLG: total lesion glycolysis; bwa: body weight-adjusted; glob4: >SUV4 method; 41pc: 41% isocontour VOI method; grad: method using a gradient-based lesion growing algorithm; SD: standard deviation; PPV: positive predictive value; NPV: negative predictive value; HR: Hazard ratio; CI: confidence interval

Table 13. Cut-off values, areas-under-the-curve (AUCs), diagnostic performance and univariate Cox-regression analyses of interim PET parameters

	DS	**ΔSUV_{max}**	**mqPET**	**rPET**
Cut-off	*1-3 / 4-5**	*-71.22%*	*1.32*	*1.54*
AUC		0.66	0.73	0.71
Sensitivity	59.3%	48.1%	59.2%	55.6%
Specificity	83.8%	85%	87.5%	92.5%
PPV	55.2%	52%	61.5%	71.4%
NPV	85.9%	82.9%	86.4%	86%
Accuracy	77.6%	75.7%	80.4%	83.2%
HR (95% CI)**	5.7 (2.6-12)	4.1 (1.9-8.8)	6.7 (3.1-14)	9.1 (4.2-20)
p**	<0.001	<0.001	<0.001	<0.001

*: according to the Lugano criteria (20); **: univariate Cox-regression analysis; PPV: positive predictive value; NPV: negative predictive value; HR: Hazard ratio; CI: confidence interval

Preserving the risk-labelling according to the ROC-analysis optimum (or the conventional values in case of DS) in the whole cohort, the predictive values were investigated of the above interim PET parameters according to clinical stage. NPV of DS, ΔSUV_{max}, mqPET, and rPET was 84.4%, 93.8%, 97.1%, and 94.6% for early stage and 82.2%, 80.0%, 82.6%, and 83.7% for advanced stage, respectively. PPV of DS, ΔSUV_{max}, mqPET, and rPET was 50.0%, 38.4%, 60.0%, and 62.5% for early stage and 58.8%, 66.7%, 62.5%, and 76.9% for advanced stage, respectively.

A similar analysis of the interim PET parameters was performed according to R-IPI scores. NPV of DS, ΔSUV_{max}, mqPET, and rPET was 92.3%, 90.6%, 92.6%, and 91.4% for patients with R-IPI scores 0-2 (n=72) and 80.8%, 75.9%, 81.5%, and 82.1% for patients with R-IPI scores 3-5 (n=35), respectively. PPV of DS, ΔSUV_{max}, mqPET, and

rPET was 45.0%, 42.1%, 50.0%, and 57.1% for patients with R-IPI scores 0-2 (n=72) and 77.8%, 75.9%, 87.5%, and 100.0% for patients with R-IPI scores 3-5 (n=35), respectively.

20 patients had an interim PET-response classified as DS4. Of them, 11 showed progression despite frontline treatment and all but one of these patients had high (exceeding the ROC-optimum of 1.54) rPET values. Thus, among the DS4 subgroup, rPET evaluation had a NPV of 87.5% and a PPV of 90.9%. In the DS4 group, NPV was 60.0% and 80.0% and PPV was 77.8% and 66.7% for ΔSUV_{max} and mqPET, respectively.

4.1.4. Combined analysis

Dividing the patients into two groups according to calculated ROC-based optimal cut-offs (or predefined, conventional values in case of DS) resulted in significantly different PFS for baseline volumetric (MTV, bwaMTV, TLG, bwaTLG), as well as interim PET parameters (DS, ΔSUV_{max}, mqPET, and rPET).

In a multivariate Cox-regression model including DS (1-3 vs. 4-5), ΔSUV_{max}, rPET, MTV, and clinical stage (early vs. advanced) only rPET was a significant independent predictor of PFS (p=0.041; HR=9.15) (Figure 4).

A combined analysis was performed by forming four groups according to low/high MTVglob4 and DS 1-3 vs. 4-5. Kaplan-Meier curves showed a good survival rate for DS1-3 patients and poor PFS for DS4-5 patients, irrespective of MTVglob4 (Figure 5a).

Furthermore, a similar combined analysis with low/high ΔSUV_{max} and low/high MTVglob4 groups resulted in relatively good PFS for all patients with low ΔSUV_{max} (irrespective of MTVglob4) and patients with high ΔSUV_{max} and low MTVglob4, while high ΔSUV_{max} patients with high MTVglob4 formed a group with distinctly poor PFS (35%) where 11 of 17 patients showed progression within two years (Figure 5b).

The majority of above results was published in Nuclear Medicine Communications in 2023 (155).

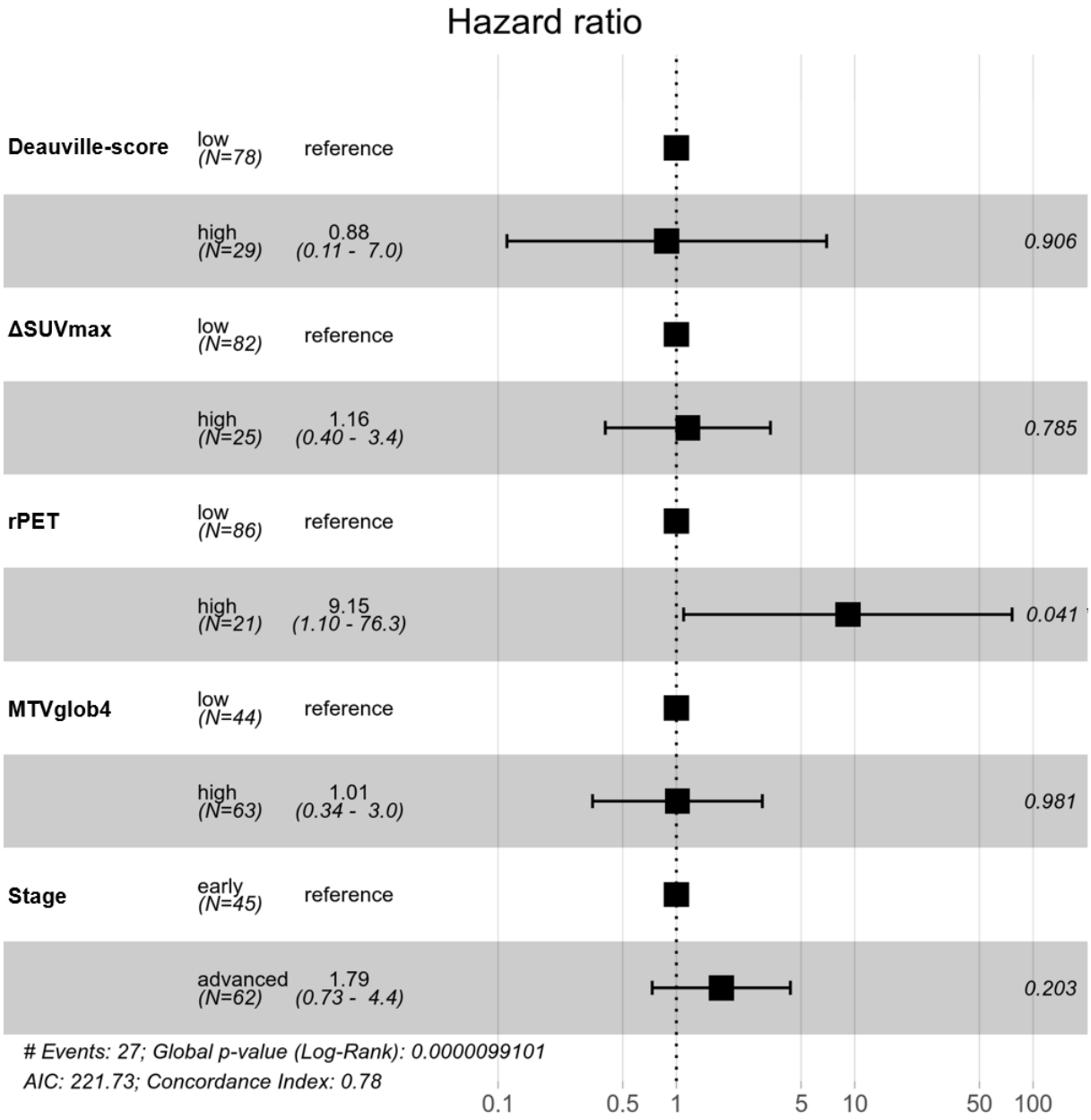

Figure 4. Multivariate Cox-regression model of progression-free survival including Deauville-score, ΔSUV_{max}, rPET, MTV, and clinical stage

SUV_{max}: maximum standardised uptake value; rPET: ratio PET; MTV: metabolic tumour volume

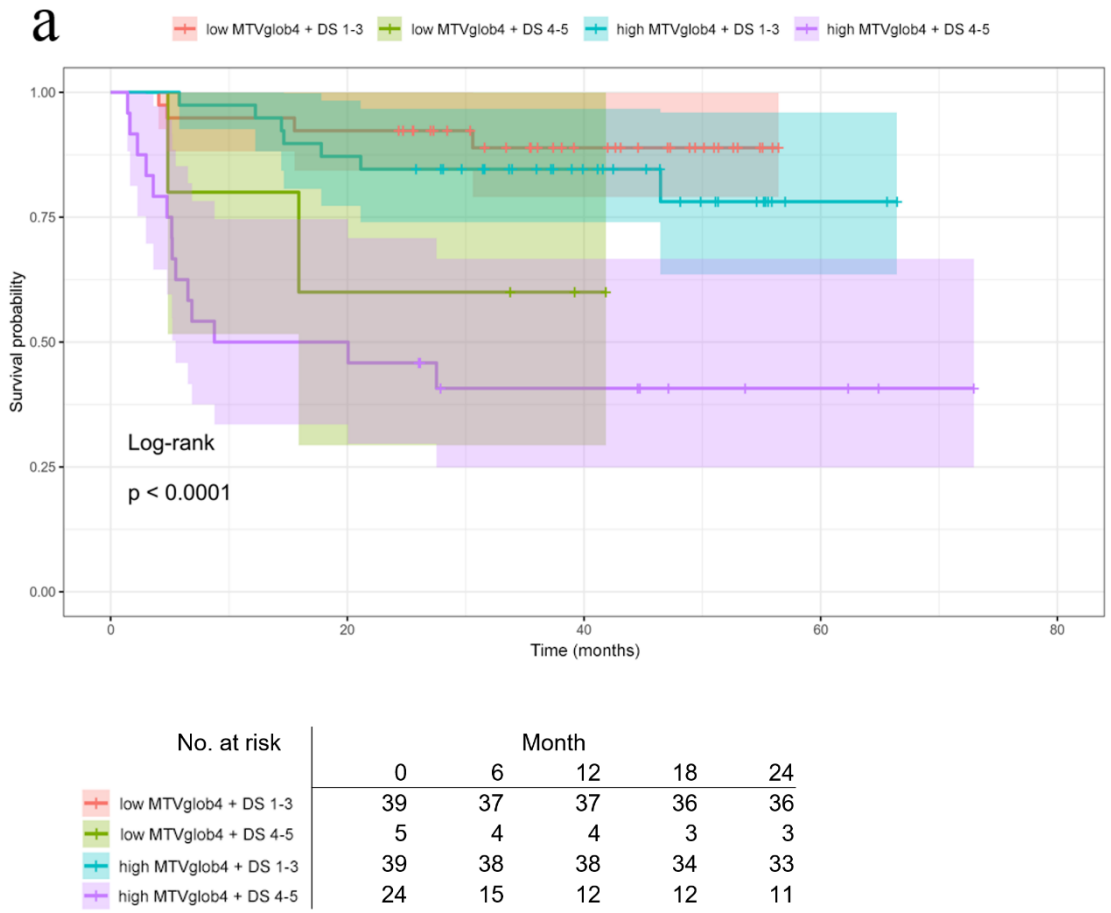

Figure 5a. Kaplan-Meier curves of progression-free survival of four subgroups according to low/high MTV and DS 1-3 vs. 4-5

MTV: metabolic tumour volume; DS: Deauville-score

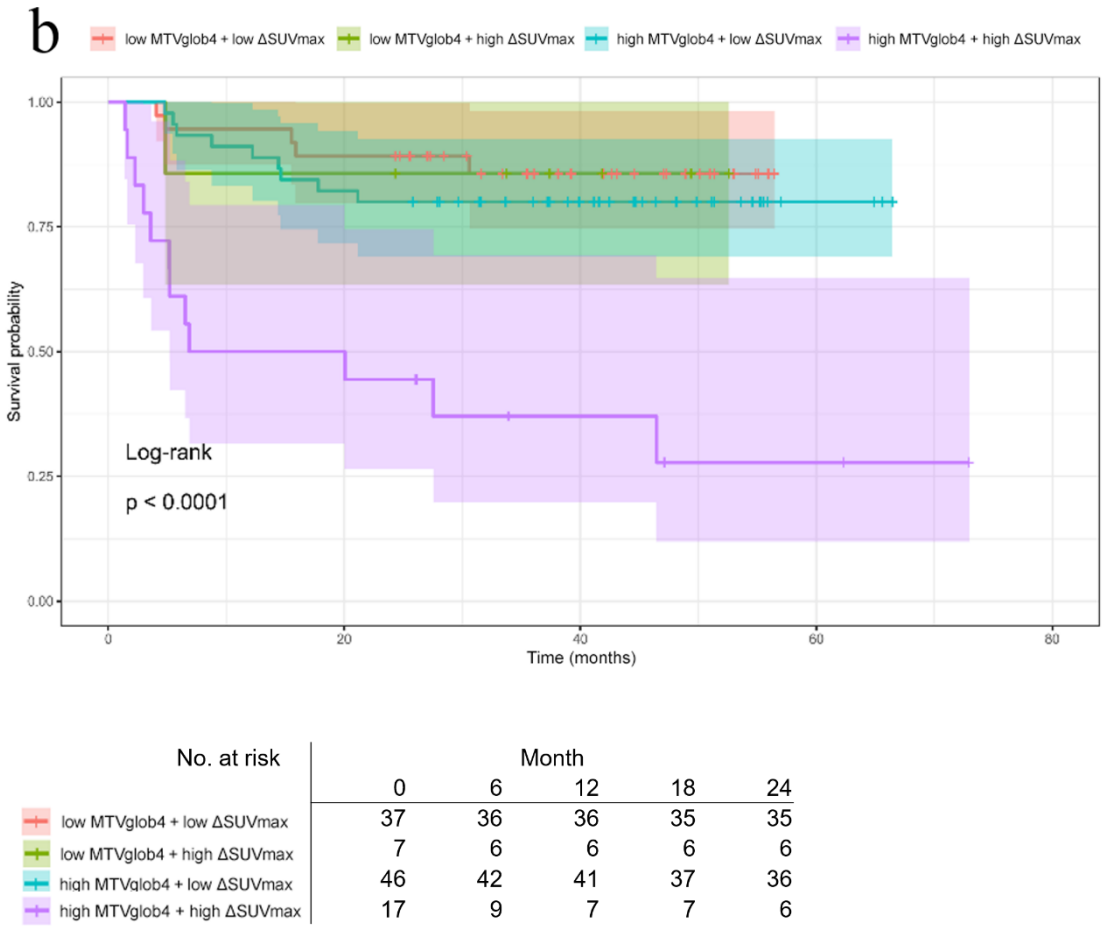

Figure 5b. Kaplan-Meier curves of progression-free survival of four subgroups according to low/high MTV and low vs. high ΔSUV_{max}

MTV: metabolic tumour volume; SUV_{max}: maximum standardised uptake value

4.2. Volumetric and textural analysis of PET/CT in patients with DLBCL, introducing the importance of novel MTVrate feature

4.2.1. Clinical and volumetric data

The investigated group consisted of 50 DLBCL NOS patients with the majority (78%) suffering from advanced (stage III and IV) disease. According to the R-IPI classification, no patient had very good prognostic score while good and poor prognostic estimations were nearly even (48% and 52%, respectively). Table 14 presents further demographic and clinical data.

4.2.2. Prognostic ability of clinical and volumetric features

Patients with early vs. advanced stage disease did not show significantly different PFS on log-rank analysis (91% vs. 72%; p=0.185), despite this dichotomic classification presenting an AUC of 0.60.

However, the phenotypic status of the DLBCL showed a significant impact on PFS as patients with GC phenotype had better prognosis than the non-GC group (PFS: 94% vs. 67%; p=0.038).

Among the investigated clinicopathological and volumetric parameters, relatively high prognostic performance on ROC analyses were observed with LDH levels (AUC=0.68), MTV (AUC=0.63), and TLG (AUC=0.63).

Patients with MTV values below or above the ROC-analysis-based optimal cut-off of 378.5 cm^3 showed significantly different 24-month PFS (94% for low-MTV vs. 68% for high-MTV groups; p=0.036).

Remarkably, the newly introduced parameter of MTVrate provided the highest AUC value at 0.74 on ROC analysis among the investigated clinical and volumetric parameters and could divide patients into low- and high-risk groups at log-rank analysis along its ROC-based optimum cut-off of 0.60 (PFS 91% vs. 50%; p<0.001) as seen in Figure 6.

Combining MTV and MTVrate data, a subgroup with particularly low PFS at 38% could be identified where patients had high MTV and low MTVrate (Figure 6).

Table 14. Patient characteristics and clinical data

Characteristic		**n= 50 (100%)**
Sex	Male	27 (54%)
	Female	23 (46%)
Age	Range	20-83 years
	Median	67 years
	> 60 years	35 (70%)
Histopathologic status	GC	17 (34%)
	non-GC	33 (66%)
Stage	I	3 (6%)
	II	8 (16%)
	III	8 (16%)
	IV	31 (62%)
R-IPI	Very good (score: 0)	0 (0%)
	Good (score: 1-2)	24 (48%)
	Poor (score: 3-5)	26 (52%)
LDH	Normal	17 (34%)
	Elevated	33 (66%)

GC: germinal centre B-cell; R-IPI: Revised International Prognostic Index: LDH, lactate-dehydrogenase

4.2.3. Textural features

Excluding the skewness parameter, which had an AUC of 0.55 on ROC-analysis and enabled stratification of two patient groups with significantly different PFS (68% vs. 94%; p=0.046) on log-rank analysis, the other first-, second-, and higher-order textural features did not show significant prognostic value when investigated individually.

A set of both OSEM and Q.Clear PET-reconstructions were available for 29 of the 50 included patients and comparing data acquired by the two different reconstructions showed that all first-order textural features had an ICC over 0.9 while second- and higher-order textural features showed greater variance in ICC values, but were mainly above 0.8. Detailed values of second- and higher-order textural features by different reconstructions are presented in Table 15.

4.2.4. Combined analysis with machine learning

The machine learning-based model, which incorporated clinical, volumetric, and textural values, assigned the greatest relative significance to the textural features contrast, long-zone low grey-level emphasis (LZLGE), zone percentage, skewness, and maximum lesion diameter (Dmax). Regarding volumetric features, both MTV and MTVrate were retained in the model as significant predictors of 24-month PFS.

Among clinical parameters, LDH levels, spleen involvement, and patient age were found to have lesser importance in the model.

By applying the model for prognosis evaluation, the AUC on ROC analysis achieved a value of 0.83 (Figure 7). By maximising the combined sensitivity and specificity on the ROC curve, a cut-off point was identified that provided a sensitivity of 66.7% and specificity of 100%.

The majority of above results was published in Nuclear Medicine Communications in 2024 (156).

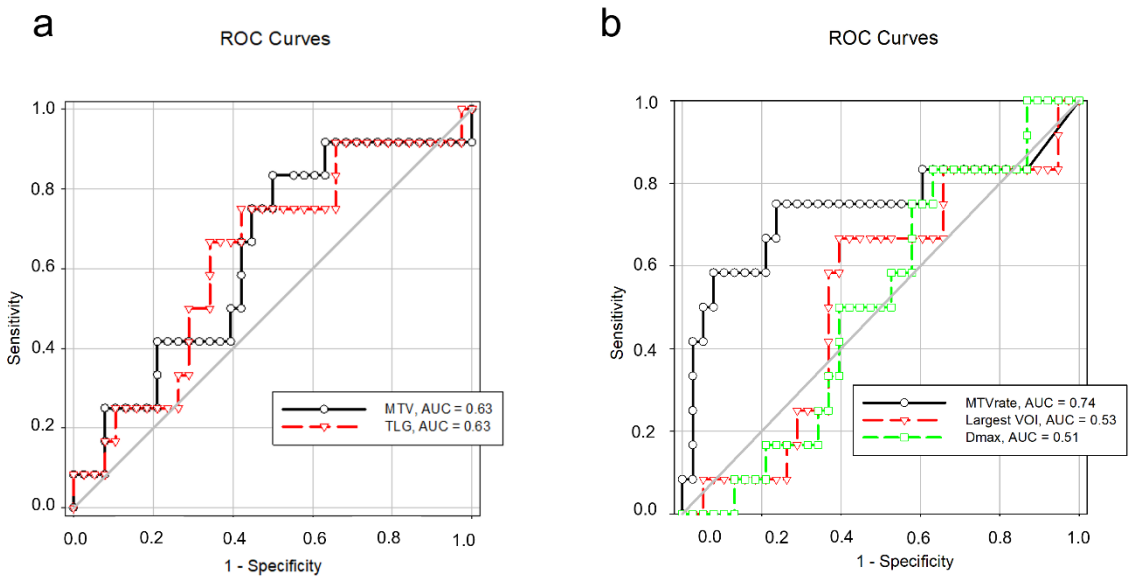

Figure 6a-b. Receiver operating characteristic curves for 24-month progression-free survival (PFS) for a) metabolic tumour volume (MTV) and total lesion glycolysis (TLG); b) MTVrate, maximum lesion volume (Largest VOI), and maximum lesion diameter (Dmax).

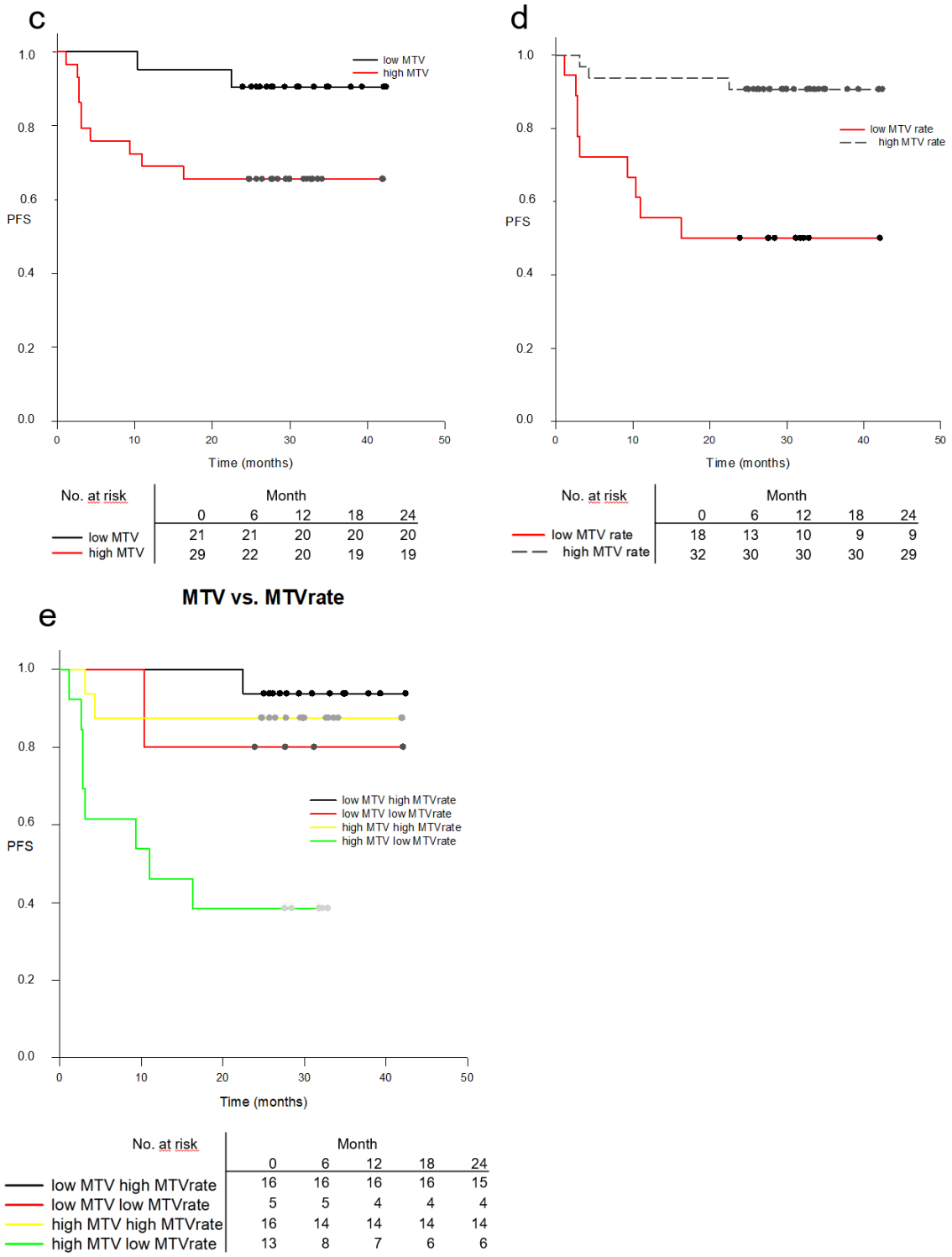

Figure 6c-e. Kaplan-Meier curves of progression-free survival between low- and high-risk patient groups divided according to c) MTV; d) MTVrate; e) MTV and MTVrate combined.

Table 15. Intraclass correlation coefficients (ICCs) of second- and higher-order textural features between two different PET-reconstructions

Textural feature	**ICC**	**95% CI**	**Textural feature**	**ICC**	**95% CI**
Entropy	0.96	0.91-0.98	Correlation	0.83	0.67-0.92
Homogeneity	0.96	0.93-0.98	Contrast	0.87	0.73-0.93
Intensity variance	0.90	0.81-0.95	Size variance	0.80	0.61-0.90
Skewness	0.91	0.82-0.96	Kurtosis	0.74	0.51-0.87
Coarseness	0.92	0.83-0.96	Complexity	0.77	0.56-0.88
Busyness	0.98	0.96-0.99	Short-zone emphasis	0.89	0.80-0.95
High grey-level zone emphasis	0.94	0.87-0.97	Low grey-level zone emphasis	0.81	0.63-0.91
Short-zone high grey-level emphasis	0.93	0.85-0.96	Short-zone low grey-level emphasis	0.73	0.50-0.86
Zone-length non-uniformity	0.90	0.81-0.95	Long-zone low grey-level emphasis	0.73	0.50-0.86
Short-run emphasis	0.95	0.89-0.97	Run percentage	0.74	0.53-0.87
Long-run emphasis	0.94	0.88-0.97	Long-zone emphasis	0.55	0.28-0.76
Low grey-level run emphasis	0.92	0.83-0.96	Long-zone high grey-level emphasis	0.72	0.49-0.86
High grey-level run emphasis	0.94	0.87-0.97	Grey-level non-uniformity	0.80	0.61-0.90
Short-run high grey-level emphasis	0.91	0.81-0.95	Zone percentage	0.81	0.64-0.91
Long-run high grey-level emphasis	0.94	0.89-0.97	Short-run low grey-level emphasis	0.66	0.39-0.82
Run length non-uniformity	0.93	0.86-0.97	Long-run low grey-level emphasis	0.88	0.77-0.94

CI: confidence interval

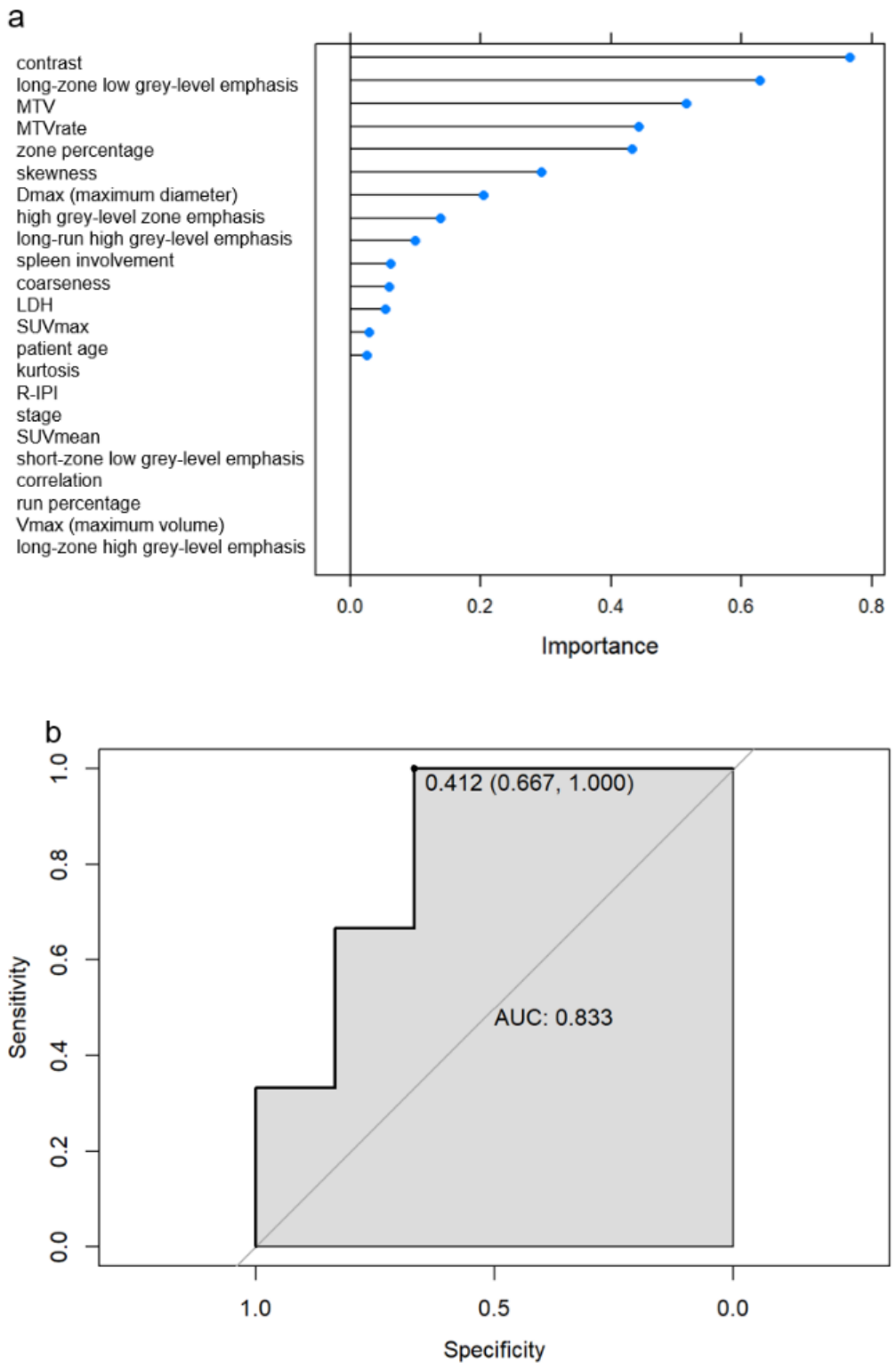

Figure 7. Results of the machine learning-based model for prognostic analysis: a) importance of different parameters within the model; b) receiver operating characteristic curve for 24-month progression-free survival.

5. DISCUSSION

5.1. Prognostic parameters on baseline and interim FDG-PET/CT in DLBCL patients

In the present study, analysis of homogenous, prospectively collected data was performed with the investigation of biomarkers from baseline and interim PET/CT scans in DLBCL patients.

5.1.1. Different segmentations of MTV

Several different methods have been described for the segmentation of MTV as shown in Table 5. The dependency of MTV values on the segmentation method has been investigated by Zhuang *et al.* in 10 non-small cell lung cancer patients, as well as by Tutino *et al.* in 121 and by Kanoun *et al.* in 59 Hodgkin's lymphoma patients, respectively (157-159). The latter two studies highlighted some slight variability not only between segmentation methods but also between softwares using the same threshold and also suggested an excellent inter-observer reproducibility across the utilised methods (158, 159). It has been suggested that the 41% isocontour-based method (referred to as 41pc in my own research) is prone to tumour FDG-uptake heterogeneity while fixed SUV-based methods (e.g. SUV≥4.0; glob4 in my research) are influenced by the variability of liver- and blood-pool SUV in multicentre setting (159-161).

Regarding DLBCL, Ilyas *et al.* investigated MTV segmented by the SUV≥2.5, the 41% isocontour, and the 'PERCIST' (≥1.5 x mean SUV + 2 standard deviations in a 3 cm^3 right liver lobe VOI) methods in 147 baseline PET/CT scans and found that all three segmentation methods were able to predict PFS and OS with similar accuracy but yielded different optimal cut-off points, as for predicting PFS, ranging 166-400 cm^3 (76). More recently, Burggraaff *et al.* suggested to use the SUV≥4.0 method after excluding all volumes less than 3.0 cm^3 in their analysis of 12 baseline PET/CT scans of DLBCL patients (77). The SUV≥4.0 method was also endorsed by a study investigating the PET/CT scans of a cohort of 140 DLBCL patients by six different methods, alongside the

‘majority vote 2’ algorithm segmenting voxels detected by at least two methods (81). Introducing a novel prognostic index including MTV, Mikhaeel *et al.* investigated PET/CT scans of a pooled cohort of 1241 DLBCL patients from five prospective research studies (84). MTV segmentation was also performed by the SUV≥4.0 method and the median MTV was 307.9 cm^3 which served as the knot of a linear spline model determining survival risk (84).

In our study, the comparison of lymphoma MTV segmentation by three different methods showed different individual volumes as presented in Table 11 and optimal cut-off points for predicting PFS with the latter value ranging 123-345 cm^3, which are comparable to those of described by Ilyas *et al.* (76). Our data showed the best agreement between the 41pc and the grad methods and the highest discrepancy between the glob4 and the 41pc segmentations (Table 10). Interestingly, these differences disappeared at the TLG values by different segmentations, most likely due to the added multiplication factor of lesion SUV_{mean}.

In addition to the variation of optimal cut-off points within the same group of patients, MTV also exhibits sample-dependency which is evident from the markedly different values obtained in studies that use the same or very similar segmentation methods, as demonstrated in the meta-analyses conducted by Xie *et al.* and Guo *et al*. where the optimal cut-off points for the SUV≥2.5 method ranged from 66 to 601.2 cm^3, while for the 40-41% methods, the range was between 16.1 and 550 cm^3 (72, 83, 85, 102, 162-168). This sample-dependency may partly explain the only moderately promising prognostic performance on ROC analyses of MTV and TLG in our data. Among the three investigated segmentation methods in our study, the gradient-based (grad) one yielded the best values, especially in terms of sensitivity and diagnostic accuracy (Table 11). However, as this latter algorithm is vendor-specific, its widespread use might be limited. Furthermore, TLG did not have better prognostic performance than MTV with the corresponding segmentation methods (Tables 11-12).

5.1.2. Body weight-adjusted MTV and TLG

The study reported in this thesis was the first to introduce body weight-adjusted (bwa) MTV and TLG values. The purpose of implementing this normalisation was to facilitate a personalised and more precise assessment of the influence of tumour burden. While normalising to body surface area or lean body mass could also be considered, our existing dataset lacked patient height information in some cases, rendering such calculations unattainable. Although bwaMTV and bwaTLG did not provide better prognostic values compared to MTV and TLG, respectively, there were a few specific cases where bwaMTV correctly categorised the patient into the appropriate risk group, unlike regular MTV (Figure 8). These novel values could be further investigated in larger cohorts as their calculation can be easily carried out.

5.1.3. Interim PET parameters

The prognostic significance of ΔSUV_{max} has been prominent in recent years, with most research identifying optimal cut-off points around 66% at I-PET2 to which our finding of 71.22% (in absolute value) is in close proximity (99, 106, 110). Curiously, our investigation found that ΔSUV_{max} did not yield more accurate prognostic information compared to the visual Deauville-score approach which supports the findings of prospective studies by Mikhaeel *et al.* and Mamot *et al.* (103, 111), but contradicts the similarly prospectively gained results of Dührsen *et al.*, Casasnovas *et al.*, and Schöder *et al.* (112, 169, 170). This latter controversy highlights the dependence on study sample, albeit two of the three above studies favouring ΔSUV_{max} to DS involved a considerably higher proportion of advanced stage patients (112, 170) than this present study or the ones by Mikhaeel *et al.* and Mamot *et al.* (103, 111).

In our analysis of patients with DLBCL, we found that the best cut-off threshold for mqPET, using a 1 cm^3 SUV_{peak} measurement, was 1.32. This value is quite comparable to the established qPET cut-off of 1.3 in paediatric Hodgkin's lymphoma patients (115), which was based on a 4-voxel-SUV_{peak} measurement and was also utilised in a large retrospective review of DLBCL patients in Germany (119).

The optimal cut-off for rPET in the present study was determined to be 1.54, which is higher than the values of 1.14 and 1.4 reported by Annunziata *et al.* and Toledano *et al.*, respectively (120, 121), however, it is similar to the finding of 1.6 reported by Fan *et al.* (100).

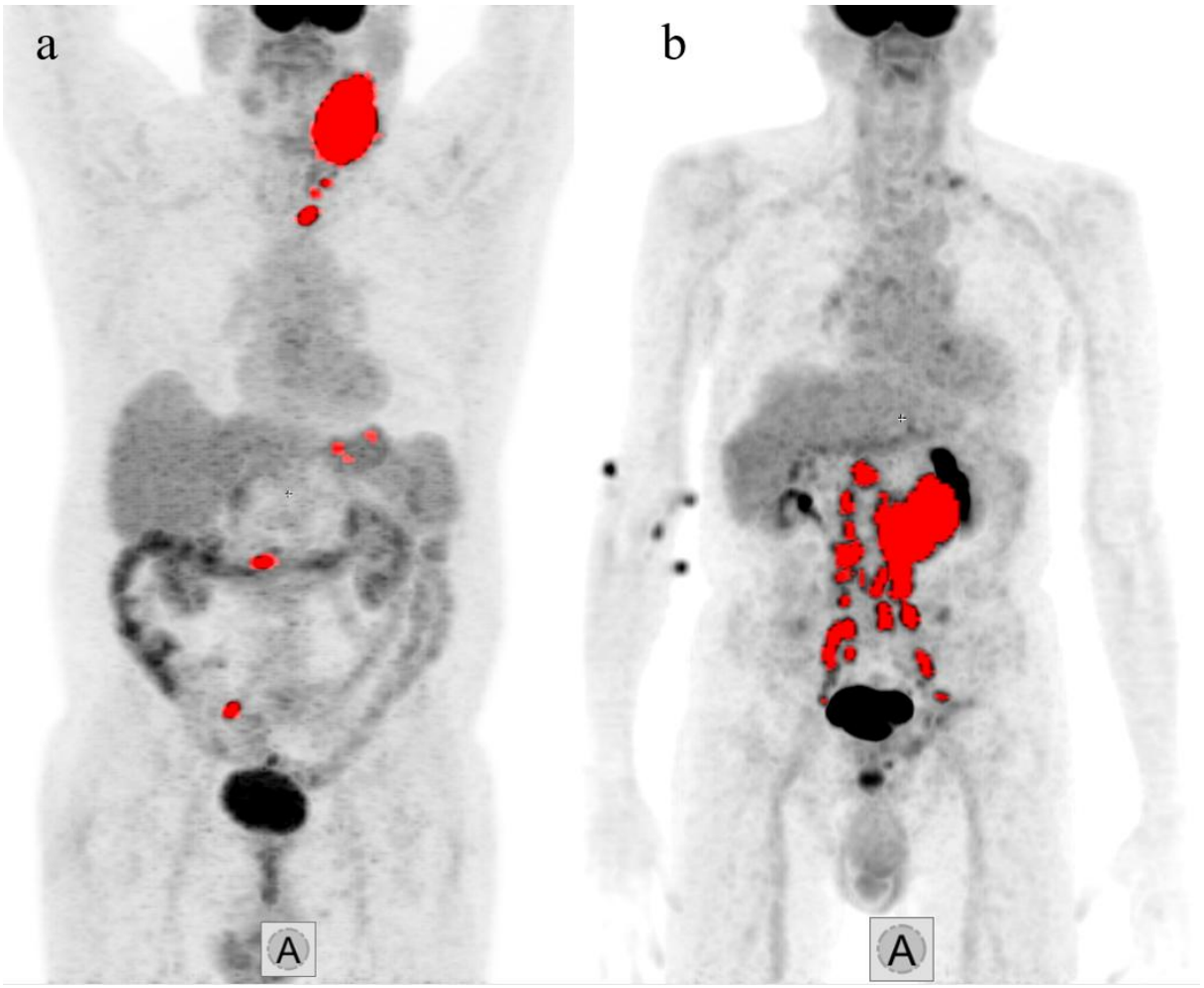

Figure 8. 3D MIP PET images with fused MTV VOIs. a) 92 kg patient with MTVglob4 of 189 cm^3 and bwaMTVglob4 of 1.76 who showed no progression during 51 months of follow-up. b) 54 kg patient with MTVglob4 of 292 cm^3 and bwaMTVglob4 of 3.16 who relapsed 7 months after baseline PET (n.b.: radiopharmaceutical skin contamination is present in the right cubital area). PET data are from the International Atomic Energy Agency Coordinated Research Project E1.50.20, display is own work.

MIP: maximum intensity projection; PET: positron emission tomography; VOI: volume of interest; MTV: metabolic tumour volume; bwaMTV: body weight-adjusted metabolic tumour volume; glob4: >SUV4 method

In the present study, univariate Cox-regression analyses underlined the excellent prognostic performance of interim parameters which markedly exceeded the hazard ratios provided by the baseline volumetric parameters and multivariate Cox-regression analysis yielded rPET as the only independent predictor of PFS.

5.1.4. Limitations of Deauville-score

DS, despite being robust and established in guidelines, is limited in full prognostic effectiveness by its inherent categorical nature as opposed to the possibilities of continuous metrics. Literature data also shows that in spite of being considered as inadequate response, DS4 often results in similar survival rates as DS1-3 in DLBCL patients at I-PET (111, 119). Based on this, it is feasible to consider a cut-off between DS4 and DS5 more appropriate, as suggested by Kurch *et al.* in the validation of qPET in DLBCL (119). The visual definition of DS4 – residual lymphoma lesion intensity exceeding the uptake of the liver parenchyma – would, in theory, translate to the continuous interim parameters as qPET, mqPET or rPET > 1.0. Data from the present study support existing findings that lower echelons of the DS4 category yield good survival rates and only residual lymphoma activity above 130%-160% of the liver uptake should be considered as inadequate treatment response, although more validation studies are required to establish a similarly robust evaluation platform as DS.

Another circumvention of the lesser prognostic effectivity of DS4 – especially to define nonresponder patients in need of treatment escalation – is to consider only DS5 as I-PET positivity (111, 119). However, the difference between DS4 and DS5 is not well circumscribed – current guidelines recommend that DS5 is applied to lesion uptake two to three times the uptake in normal liver (20, 54). In the present study, DS5 was defined as lesion SUV_{max} three times over liver SUV_{max}, as in the United Kingdom (UK) National Cancer Research Institute (NCRI) trial and thus, similarly low proportion of patients (less than 10%) showed DS5 on I-PET with these criteria (111). Mikhaeel *et al.* in a post-hoc analysis changed their DS5 criterion to residual lymphoma uptake at least twice higher than normal liver and/or new lesions, but encountered a reduction in discriminatory power (111). The value of rPET-based stratification was highlighted in the present study, as in the DS4 subgroup (n=20; 18.7% of the cohort), only 1 patient relapsed below the optimal

cut-off of 1.54 and all but one patient above the threshold showed progression, resulting in a NPV of 87.5% and a PPV of 90.9%. However, despite calls for further validation, no major DLBCL study investigated rPET so far apart from this research (171).

5.1.5. Combined analyses

Furthermore, combined analyses showed that DS1-3 on interim PET has a higher impact on PFS than baseline MTV whereas Mikhaeel *et al.* in their retrospective study of 147 DLBCL patients found that MTV≥400 cm^3 had a worse prognosis, irrespective of DS on interim scans (102). The discrepancy between our findings and the previously published results is likely attributed to sample bias. However, the multicentre nature of our study enhances the credibility of our findings. This is particularly significant because it has been demonstrated that the international diversity of the original IAEA study did not restrict the global relevance of its data (104). Also, the study by Mikhaeel *et al.* (102) contained relatively more patients with stage IV DLBCL (58%) than the present report (40%). In a wider scope, it has been showed that the majority of published studies investigating baseline MTV in DLBCL and HL are retrospective, heterogenous in methodology, underpowered, and lack standardisation (70, 78) while DS is more robust and has more powerful validation (54, 106, 172). Given the above, our finding of the superior prognostic performance of stratification by DS over MTV is feasible in the context of current scientific evidence.

Importantly, in the present study the combination of baseline MTV and ΔSUV_{max} enabled to define a group of patients with high baseline MTV and high ΔSUV_{max} on interim scan who had a particularly poor PFS of 35% which was more emphasised in the cohort investigated by Mikhaeel *et al.* where this cohort (with slightly different cut-off values for MTV and ΔSUV_{max}) had a PFS of 19% (102).

5.1.6. Prognostic values in specific risk groups

The clinical utility of interim PET-based prognostic evaluation – if sufficiently reliable – is to enable early treatment modification (96, 122). In general, high NPV is required to properly select candidates for treatment de-escalation and high PPV is the basis of

escalation or change in therapeutic regime. In the whole cohort, rPET-based risk stratification showed high NPV of 86% and a remarkably good PPV of 71.4% – the highest PPV of all examined biomarkers. Relapse or progression is less common among patients with early stage DLBCL, thus this cohort is more likely to give candidates for de-escalation (24). In that regard, the high NPV of bwaTLG41pc (96.3%) and mqPET (97.1%) among early-stage patients can serve as a basis of patient selection for de-escalation. Similarly, the high PPV of rPET of 76.9% in the advanced stage subgroup can help identify candidates for escalation strategies.

Similarly, among patients with very good and good R-IPI (scores 0-2), NPV was highest for bwaTLGgrad and remained above 90% for DS, ΔSUV_{max}, mqPET, and rPET. Interestingly, patients with poor R-IPI classification (scores: 3-5) had a 100% PPV with rPET-based classification which has a considerable potential in adequate candidate selection for treatment escalation, especially as I-PET2–based treatment escalation has not yet been effective in DLBCL (95, 169). So far, the only major, phase 3 trial proving the possibility of treatment de-escalation has not included I-PET-based classification factors, only conventional risk factors as age<60 years, early stage disease, normal serum LDH levels, Eastern Cooperative Oncology Group (ECOG) performance status 0–1, and no bulky disease (maximum tumour diameter<7.5 cm) served as the inclusion criteria (173).

5.2. Volumetric and textural analysis of PET/CT in patients with DLBCL, introducing the importance of novel MTVrate feature

A retrospective analysis of baseline PET data was conducted to assess prognosis in DLBCL patients, and it was found that individual assessment of various clinical, volumetric, and textural biomarkers yielded limited prognostic data, but implementing a machine learning-based combined analysis was remarkably effective.

5.2.1. Value of MTVrate and conventional volumetric PET parameters

MTVrate – the quotient of the volume of the greatest lesion and the total body MTV – was first described in the scientific literature by our workgroup (156). In our investigated group of 50 DLBCL patients, MTVrate had the highest prognostic value among the individually investigated volumetric and clinical parameters (AUC=0.74).

Unexpectedly, lower MTVrates yielded poorer prognosis and, suggesting that the presence of multiple, comparatively smaller, dispersed lymphoma lesions was more detrimental than a large lesion surrounded by few or no smaller ones. The clinical context requires further validation, but one assumption could be a hypothetical association between higher stage and more scattered disease. This could not be proven in out cohort, as the patients with low MTVrate values (posing high-risk) only encompassed 41% (16/39) of the advanced-stage subgroup.

MTVrate in itself is a ratio that does not consider the precise size of lymphoma lesions, but when coupled with total-body MTV, it could be utilised to reveal a patient subgroup with a notably low 24-month PFS of 38%.

Like many prior trials, ROC-optimised patient risk classification of MTV led to groups with markedly varied PFS (83, 85, 162, 163), but within our group of patients, the predictive performance of MTV and TLG was only marginally promising and even LDH levels yielded higher prognostic values on ROC-analysis.

5.2.2. Impact of textural analysis

Reconstruction algorithm, among other technical parameters, can influence textural feature data (174, 175). In our subanalysis, first-order textural features exhibited strong correlation; however, approximately half of the examined second- and higher-order radiomic features displayed significant discrepancies in values between PET reconstructions utilising either the conventional OSEM method or the relatively novel Bayesian penalised likelihood-based algorithm (Q.Clear).

In the analysis of individual textural features, only skewness demonstrated significant differentiating capability in prognostic assessment. The integrated machine learning

model primarily included second- and higher-order textural features as significant predictive biomarkers, along with MTV and MTVrate, while certain clinical factors held lesser importance. This model had excellent prognostic capability, with an AUC of 0.83 in ROC analysis.

Importantly, in a multivariate prediction model, correlated variables that provide overlapping information do not necessarily contribute additional predictive power. For example, R-IPI already incorporates age and LDH, both of which have predictive value on their own, so including R-IPI in the same model may not improve prediction further (as can be seen in Figure 7b, where R-IPI had virtually no added predictive capability). A similar principle applies to MTV and MTVrate: because they are correlated, their relative predictive influence can shift when analysed together rather than individually. Moreover, univariate ROC curves serve as descriptive statistics, whereas the multivariate model is specifically trained on a portion of the data to optimize prediction and then tested on unseen data. Consequently, since the purpose of the predictive model differs from that of the descriptive ROC curves, the variables' relative importance can also change.

In 2020, Aide *et al.* performed a study involving 132 DLBCL patients, analysing the individual prognostic efficacy of conventional and textural measures where patients were allocated into teaching and validation groups in a ratio of 105 to 27 (144). In ROC analysis, long-zone high grey-level emphasis (LZHGE) emerged as the superior higher-order variable, achieving the highest AUC of 0.69 and it was the sole independent predictor of 24-month PFS in Cox survival analysis (142). Additionally, in log-rank analysis, MTV, 4 second-order, and 5 higher-order features (including LZHGE) showed differentiating power for 24-month PFS (142).

In 2021, Coskun *et al.* employed analogous methods to develop a predictive model for estimating patient outcomes based on a sample size comparable to ours (148). A cohort of 45 DLBCL patients was analysed using elastic net regularisation logistic regression for model development, employing 3-fold cross-validation for training. The fundamental distinction between the study and ours was the methodology employed in preparing the study sample. VOIs were established based on a threshold of SUV_{max} > 40%, and the parameters for evaluation were derived from the 6 biggest lesions of each patient, or fewer if applicable, utilising texture and SUV-based metrics (148). Their research revealed that

SUV_{max} and GLCM dissimilarity were independent predictors of 24-month PFS, with their model demonstrating an AUC of 0.81 in ROC analysis (148). It is noteworthy that, within a comparable sample size and analogous model design, our prediction accuracy was shown to be identical despite the differing data gathering methods.

Eertink *et al.* investigated baseline PET scans of 317 newly diagnosed DLBCL patients and discovered that a model incorporating tumour-related parameters (MTV, SUV_{peak}, and $Dmax_{bulk}$ [the distance between the two most distant lymphoma lesions]) and patient-related factors (WHO performance status and age over 60 years) exhibited the highest prognostic capability, achieving an AUC of 0.79 (150). A larger, pooled cohort was later used to validate these results (154).

Our study has some limitations. Initially, our research was retrospective; however, by incorporating consecutive patients undergoing baseline PET/CT in our department, the data may reflect real-world practice. Secondly, the limited patient population and the plethora of diverse clinical, volumetric, and textural biomarkers presented a risk of overfitting in our machine learning model, which we attempted to mitigate through the application of elastic net regularisation. Thirdly, additional information accumulates about the significance of the molecular heterogeneity of DLBCL, our lack of molecular genetic data diminishes the robustness of our combined model (16, 17, 176).

6. CONCLUSIONS

6.1. Prognostic parameters on baseline and interim FDG-PET/CT in DLBCL patients

The baseline MTV values and optimal cut-off points obtained by various segmentation methods exhibited significant variation and demonstrated only minor prognostic significance in our multicentric investigation of DLBCL patients. This was the inaugural publication of body weight-adjusted MTV and TLG values and although these values did not demonstrate significantly enhanced prognostic capability over their conventional (non-normalised) counterparts, there were a limited number of instances where body weight-adjusted MTV accurately classified the patient into the appropriate risk group, unlike standard MTV.

Interim PET/CT parameters yielded more precise prognostic information compared to baseline volumetric data, with semiquantitative "Deauville-like" metrics (most notably, rPET) demonstrating superior performance in this trial over conventional visual response evaluation (DS). The integration of baseline MTV and ΔSUV_{max} facilitated the differentiation of a patient cohort with notably adverse prognosis.

6.2. Volumetric and textural analysis of PET/CT in patients with DLBCL, introducing the importance of novel MTVrate feature

Our retrospective analysis of baseline PET data to assess the prognosis of patients with DLBCL revealed that the individual assessment of various clinical, volumetric, and textural biomarkers provided limited prognostic information, whereas a machine learning-based integrated analysis demonstrated high efficacy.

The newly established MTVrate, calculated as the ratio of the largest lesion's volume to total body MTV, had the greatest predictive capability in individual assessments and, when paired with MTV, facilitated the identification of a patient cohort with notably adverse prognosis.

7. SUMMARY

Objective: To investigate potential roles of existing [^{18}F]FDG-PET/CT prognostic parameters in DLBCL and to establish new or modified methods which are both easy to implement in routine workflows and yield more accurate results than the current ones.

Methods: First, data of 107 DLBCL NOS patients from a multicentre, prospective trial were used for analysis of baseline volumetric values (MTV and TLG, also normalised for body weight) segmented with three different methods and interim parameters. Secondly, retrospective analysis of 50 baseline PET/CT scans from one centre was performed to investigate textural PET features and the newly defined MTVrate value, alongside MTV and clinical data, including prognostic model-building utilizing a machine learning algorithm. 24-month PFS was the clinical endpoint at both studies and ROC analyses were performed to define optimal cut-off points for continuous parameters. The PFS of low- and high-risk groups were compared with log-rank and Cox-regression analysis.

Results: In the analysis of the multicentre data, MTV and TLG calculations showed good correlation among the three segmentation methods, however, optimal cut-off points were markedly different. Body weight-adjusted MTV and TLG did not provide markedly better prognostic values. Highest hazard ratio was shown for rPET (HR=9.09) and it was also shown to be an independent predictor of PFS (p=0.041; HR=9.15) in a multivariate Cox-regression model. A combined analysis showed that patients with high ΔSUV_{max} and high MTV formed a group with distinctly poor PFS (35.3%). Among the single-centre data, individual analysis showed the highest AUC on ROC analysis for MTVrate at 0.74, followed by LDH, MTV, and skewness, with AUCs of 0.68, 0.63, and 0.55, respectively, and these parameters were also able to differentiate the PFS. A combined analysis including MTV and MTVrate identified a subgroup with particularly low PFS at 38%. The machine learning-based model had an AUC of 0.83 and the highest relative importance was attributed to five textural features and both MTV and MTVrate.

Conclusion: Results from the analysis of both datasets underline the importance of FDG-PET/CT in the prognostic evaluation of DLBCL patients and indicate PET-based markers that are highly effective and easily implementable in routine clinical practice: MTV and the novel MTVrate feature at baseline and rPET at interim PET.

8. REFERENCES

1. Bray F, Ferlay J, Soerjomataram I, Siegel RL, Torre LA, Jemal A. Global cancer statistics 2018: GLOBOCAN estimates of incidence and mortality worldwide for 36 cancers in 185 countries. CA: A Cancer Journal for Clinicians. 2018;68(6):394-424.
2. Thandra KC, Barsouk A, Saginala K, Padala SA, Rawla P. Epidemiology of Non-Hodgkin's Lymphoma. Med Sci (Basel). 2021;9(1).
3. Li S, Young KH, Medeiros LJ. Diffuse large B-cell lymphoma. Pathology. 2018;50(1):74-87.
4. Sukswai N, Lyapichev K, Khoury JD, Medeiros LJ. Diffuse large B-cell lymphoma variants: an update. Pathology. 2020;52(1):53-67.
5. de Leval L, Jaffe ES. Lymphoma Classification. Cancer journal (Sudbury, Mass). 2020;26(3):176-85.
6. Martelli M, Ferreri AJ, Agostinelli C, Di Rocco A, Pfreundschuh M, Pileri SA. Diffuse large B-cell lymphoma. Crit Rev Oncol Hematol. 2013;87(2):146-71.
7. Campo E, Harris NL, Jaffe ES, Pileri SA, Stein H, Thiele J. WHO Classification of Tumours of Haematopoietic and Lymphoid Tissues: International Agency for Research on Cancer; 2017.
8. Susanibar-Adaniya S, Barta SK. 2021 Update on Diffuse large B cell lymphoma: A review of current data and potential applications on risk stratification and management. Am J Hematol. 2021;96(5):617-29.
9. Hartge P, Wang S. Overview of the etiology and epidemiology of lymphoma. Non-Hodgkin’s lymphomas. 2004;11:711-27.
10. Vianna N. The malignant lymphomas: epidemiology and related aspects. Pathobiology annual. 1977;7:231-55.
11. Tilly H, Gomes da Silva M, Vitolo U, Jack A, Meignan M, Lopez-Guillermo A, et al. Diffuse large B-cell lymphoma (DLBCL): ESMO Clinical Practice Guidelines for diagnosis, treatment and follow-up. Ann Oncol. 2015;26 Suppl 5:v116-25.
12. Alizadeh AA, Eisen MB, Davis RE, Ma C, Lossos IS, Rosenwald A, et al. Distinct types of diffuse large B-cell lymphoma identified by gene expression profiling. Nature. 2000;403(6769):503-11.

13. Johnson NA, Savage KJ, Ludkovski O, Ben-Neriah S, Woods R, Steidl C, et al. Lymphomas with concurrent BCL2 and MYC translocations: the critical factors associated with survival. Blood. 2009;114(11):2273-9.
14. Savage KJ, Johnson NA, Ben-Neriah S, Connors JM, Sehn LH, Farinha P, et al. MYC gene rearrangements are associated with a poor prognosis in diffuse large B-cell lymphoma patients treated with R-CHOP chemotherapy. Blood. 2009;114(17):3533-7.
15. Schmitz R, Wright GW, Huang DW, Johnson CA, Phelan JD, Wang JQ, et al. Genetics and Pathogenesis of Diffuse Large B-Cell Lymphoma. N Engl J Med. 2018;378(15):1396-407.
16. Chapuy B, Stewart C, Dunford AJ, Kim J, Kamburov A, Redd RA, et al. Molecular subtypes of diffuse large B cell lymphoma are associated with distinct pathogenic mechanisms and outcomes. Nat Med. 2018;24(5):679-90.
17. Wright GW, Huang DW, Phelan JD, Coulibaly ZA, Roulland S, Young RM, et al. A Probabilistic Classification Tool for Genetic Subtypes of Diffuse Large B Cell Lymphoma with Therapeutic Implications. Cancer Cell. 2020;37(4):551-68.e14.
18. Carbone PP, Kaplan HS, Musshoff K, Smithers DW, Tubiana M. Report of the Committee on Hodgkin's Disease Staging Classification. Cancer Res. 1971;31(11):1860-1.
19. Lister T, Crowther D, Sutcliffe S, Glatstein E, Canellos G, Young R, et al. Report of a committee convened to discuss the evaluation and staging of patients with Hodgkin's disease: Cotswolds meeting. Journal of Clinical Oncology. 1989;7(11):1630-6.
20. Cheson BD, Fisher RI, Barrington SF, Cavalli F, Schwartz LH, Zucca E, et al. Recommendations for initial evaluation, staging, and response assessment of Hodgkin and non-Hodgkin lymphoma: the Lugano classification. J Clin Oncol. 2014;32(27):3059-68.
21. Solal-Céligny P, Lepage E, Brousse N, Tendler CL, Brice P, Haïoun C, et al. Doxorubicin-containing regimen with or without interferon alfa-2b for advanced follicular lymphomas: final analysis of survival and toxicity in the Groupe d'Etude des Lymphomes Folliculaires 86 Trial. J Clin Oncol. 1998;16(7):2332-8.
22. Zelenetz AD, Gordon LI, Abramson JS, Advani RH, Andreadis B, Bartlett NL, et al. NCCN Guidelines® Insights: B-Cell Lymphomas, Version 6.2023. J Natl Compr Canc Netw. 2023;21(11):1118-31.

23. Boellaard R, Delgado-Bolton R, Oyen WJ, Giammarile F, Tatsch K, Eschner W, et al. FDG PET/CT: EANM procedure guidelines for tumour imaging: version 2.0. Eur J Nucl Med Mol Imaging. 2015;42(2):328-54.
24. International Non-Hodgkin's Lymphoma Prognostic Factors Project. A predictive model for aggressive non-Hodgkin's lymphoma. N Engl J Med. 1993;329(14):987-94.
25. Mikhaeel NG. Is 70 the new 60? New international prognostic index with an older age cut-off for diffuse large B-cell lymphoma. Leuk Lymphoma. 2015;56(9):2487-8.
26. Gang AO, Pedersen M, d'Amore F, Pedersen LM, Jensen BA, Jensen P, et al. A clinically based prognostic index for diffuse large B-cell lymphoma with a cut-off at 70 years of age significantly improves prognostic stratification: population-based analysis from the Danish Lymphoma Registry. Leuk Lymphoma. 2015;56(9):2556-62.
27. Sehn LH, Berry B, Chhanabhai M, Fitzgerald C, Gill K, Hoskins P, et al. The revised International Prognostic Index (R-IPI) is a better predictor of outcome than the standard IPI for patients with diffuse large B-cell lymphoma treated with R-CHOP. Blood. 2007;109(5):1857-61.
28. Ziepert M, Hasenclever D, Kuhnt E, Glass B, Schmitz N, Pfreundschuh M, et al. Standard International prognostic index remains a valid predictor of outcome for patients with aggressive CD20+ B-cell lymphoma in the rituximab era. J Clin Oncol. 2010;28(14):2373-80.
29. Zhou Z, Sehn LH, Rademaker AW, Gordon LI, Lacasce AS, Crosby-Thompson A, et al. An enhanced International Prognostic Index (NCCN-IPI) for patients with diffuse large B-cell lymphoma treated in the rituximab era. Blood. 2014;123(6):837-42.
30. Coiffier B, Thieblemont C, Van Den Neste E, Lepeu G, Plantier I, Castaigne S, et al. Long-term outcome of patients in the LNH-98.5 trial, the first randomized study comparing rituximab-CHOP to standard CHOP chemotherapy in DLBCL patients: a study by the Groupe d'Etudes des Lymphomes de l'Adulte. Blood. 2010;116(12):2040-5.
31. Ernst M, Dührsen U, Hellwig D, Lenz G, Skoetz N, Borchmann P. Diffuse Large B-Cell Lymphoma and Related Entities. Dtsch Arztebl Int. 2023;120(17):289-96.
32. Oken MM, Creech RH, Tormey DC, Horton J, Davis TE, McFadden ET, et al. Toxicity and response criteria of the Eastern Cooperative Oncology Group. Am J Clin Oncol. 1982;5(6):649-55.

33. Feugier P, Van Hoof A, Sebban C, Solal-Celigny P, Bouabdallah R, Fermé C, et al. Long-term results of the R-CHOP study in the treatment of elderly patients with diffuse large B-cell lymphoma: a study by the Groupe d'Etude des Lymphomes de l'Adulte. J Clin Oncol. 2005;23(18):4117-26.

34. Zelenetz AD, Gordon LI, Abramson JS, Advani RH, Andreadis B, Bartlett NL, et al. NCCN Guidelines® Insights: B-Cell Lymphomas, Version 1.2025. https://wwwnccnorg/guidelines/. 2024.

35. Yamauchi N, Maruyama D. Current treatment approach and future perspectives in B cell lymphoma. Int J Hematol. 2024.

36. Smits NC, Sentman CL. Bispecific T-Cell Engagers (BiTEs) as Treatment of B-Cell Lymphoma. J Clin Oncol. 2016;34(10):1131-3.

37. Ioannou N, Jain K, Ramsay AG. Immunomodulatory Drugs for the Treatment of B Cell Malignancies. Int J Mol Sci. 2021;22(16).

38. Rhodes J, Landsburg DJ. Small-Molecule Inhibitors for the Treatment of Diffuse Large B Cell Lymphoma. Curr Hematol Malig Rep. 2018;13(5):356-68.

39. Hamadani M, Gopal AK, Pasquini M, Kim S, Qiu X, Ahmed S, et al. Allogeneic transplant and CAR-T therapy after autologous transplant failure in DLBCL: a noncomparative cohort analysis. Blood Adv. 2022;6(2):486-94.

40. Agrawal K, Skillen A, Esmail A, Usmani S. PET/CT imaging. 1 ed. Cham, Switzerland: Springer Nature; 2021 2021/12/3. 124 p.

41. Mettler FA, Jr., Guiberteau MJ. Essentials of nuclear medicine and molecular imaging. 7 ed. Philadelphia, PA: Elsevier - Health Sciences Division; 2018 2018/11/7. 560 p.

42. Adams MC, Turkington TG, Wilson JM, Wong TZ. A systematic review of the factors affecting accuracy of SUV measurements. AJR Am J Roentgenol. 2010;195(2):310-20.

43. Aide N, Lasnon C, Veit-Haibach P, Sera T, Sattler B, Boellaard R. EANM/EARL harmonization strategies in PET quantification: from daily practice to multicentre oncological studies. Eur J Nucl Med Mol Imaging. 2017;44(Suppl 1):17-31.

44. Kaalep A, Sera T, Rijnsdorp S, Yaqub M, Talsma A, Lodge MA, et al. Feasibility of state of the art PET/CT systems performance harmonisation. Eur J Nucl Med Mol Imaging. 2018;45(8):1344-61.

45. Cook GJR, Maisey MN, Britton KE, Vaseem C. Clinical Nuclear Medicine. 4 ed. London, England: Hodder Arnold; 2006 2006/11/24. 896 p.
46. Yamada S, Kubota K, Kubota R, Ido T, Tamahashi N. High accumulation of fluorine-18-fluorodeoxyglucose in turpentine-induced inflammatory tissue. J Nucl Med. 1995;36(7):1301-6.
47. Lewis PJ, Salama A. Uptake of fluorine-18-fluorodeoxyglucose in sarcoidosis. J Nucl Med. 1994;35(10):1647-9.
48. Knopp MV, Bischoff HG. [Evaluation of pulmonary lesions with positron emission tomography]. Radiologe. 1994;34(10):588-91.
49. van der Vos CS, Koopman D, Rijnsdorp S, Arends AJ, Boellaard R, van Dalen JA, et al. Quantification, improvement, and harmonization of small lesion detection with state-of-the-art PET. Eur J Nucl Med Mol Imaging. 2017;44(Suppl 1):4-16.
50. Teoh EJ, McGowan DR, Macpherson RE, Bradley KM, Gleeson FV. Phantom and Clinical Evaluation of the Bayesian Penalized Likelihood Reconstruction Algorithm Q.Clear on an LYSO PET/CT System. J Nucl Med. 2015;56(9):1447-52.
51. Matti A, Lima GM, Pettinato C, Pietrobon F, Martinelli F, Fanti S. How Do the More Recent Reconstruction Algorithms Affect the Interpretation Criteria of PET/CT Images? Nucl Med Mol Imaging. 2019;53(3):216-22.
52. Özülker F, Babacan GB, Cengiz S, Özülker T. The effect of reconstruction algorithms on semi-quantitative measurements in. Hell J Nucl Med. 2024;27(2):85-92.
53. Schöder H, Noy A, Gönen M, Weng L, Green D, Erdi YE, et al. Intensity of 18fluorodeoxyglucose uptake in positron emission tomography distinguishes between indolent and aggressive non-Hodgkin's lymphoma. J Clin Oncol. 2005;23(21):4643-51.
54. Barrington SF, Mikhaeel NG, Kostakoglu L, Meignan M, Hutchings M, Müeller SP, et al. Role of imaging in the staging and response assessment of lymphoma: consensus of the International Conference on Malignant Lymphomas Imaging Working Group. J Clin Oncol. 2014;32(27):3048-58.
55. Elstrom R, Guan L, Baker G, Nakhoda K, Vergilio JA, Zhuang H, et al. Utility of FDG-PET scanning in lymphoma by WHO classification. Blood. 2003;101(10):3875-6.
56. Papajík T, Mysliveček M, Sedová Z, Buriánková E, Procházka V, Koranda P, et al. Standardised uptake value of 18F-FDG on staging PET/CT in newly diagnosed

patients with different subtypes of non-Hodgkin's lymphoma. Eur J Haematol. 2011;86(1):32-7.

57. Weiler-Sagie M, Bushelev O, Epelbaum R, Dann EJ, Haim N, Avivi I, et al. (18)F-FDG avidity in lymphoma readdressed: a study of 766 patients. J Nucl Med. 2010;51(1):25-30.

58. El-Galaly TC, Gormsen LC, Hutchings M. PET/CT for Staging; Past, Present, and Future. Semin Nucl Med. 2018;48(1):4-16.

59. Raanani P, Shasha Y, Perry C, Metser U, Naparstek E, Apter S, et al. Is CT scan still necessary for staging in Hodgkin and non-Hodgkin lymphoma patients in the PET/CT era? Ann Oncol. 2006;17(1):117-22.

60. Luminari S, Biasoli I, Arcaini L, Versari A, Rusconi C, Merli F, et al. The use of FDG-PET in the initial staging of 142 patients with follicular lymphoma: a retrospective study from the FOLL05 randomized trial of the Fondazione Italiana Linfomi. Ann Oncol. 2013;24(8):2108-12.

61. Juweid ME, Wiseman GA, Vose JM, Ritchie JM, Menda Y, Wooldridge JE, et al. Response assessment of aggressive non-Hodgkin's lymphoma by integrated International Workshop Criteria and fluorine-18-fluorodeoxyglucose positron emission tomography. J Clin Oncol. 2005;23(21):4652-61.

62. Dupuis J, Berriolo-Riedinger A, Julian A, Brice P, Tychyj-Pinel C, Tilly H, et al. Impact of [(18)F]fluorodeoxyglucose positron emission tomography response evaluation in patients with high-tumor burden follicular lymphoma treated with immunochemotherapy: a prospective study from the Groupe d'Etudes des Lymphomes de l'Adulte and GOELAMS. J Clin Oncol. 2012;30(35):4317-22.

63. Trotman J, Fournier M, Lamy T, Seymour JF, Sonet A, Janikova A, et al. Positron emission tomography-computed tomography (PET-CT) after induction therapy is highly predictive of patient outcome in follicular lymphoma: analysis of PET-CT in a subset of PRIMA trial participants. J Clin Oncol. 2011;29(23):3194-200.

64. Meignan M, Gallamini A, Haioun C. Report on the First International Workshop on Interim-PET-Scan in Lymphoma. Leuk Lymphoma. 2009;50(8):1257-60.

65. Fuertes S, Setoain X, López-Guillermo A, Montserrat E, Fuster D, Paredes P, et al. [The value of positron emission tomography/computed tomography (PET/CT) in the staging of diffuse large B-cell lymphoma]. Med Clin (Barc). 2007;129(18):688-93.

66. Carr R, Barrington SF, Madan B, O'Doherty MJ, Saunders CA, van der Walt J, et al. Detection of lymphoma in bone marrow by whole-body positron emission tomography. Blood. 1998;91(9):3340-6.
67. Pelosi E, Penna D, Douroukas A, Bellò M, Amati A, Arena V, et al. Bone marrow disease detection with FDG-PET/CT and bone marrow biopsy during the staging of malignant lymphoma: results from a large multicentre study. Q J Nucl Med Mol Imaging. 2011;55(4):469-75.
68. Berthet L, Cochet A, Kanoun S, Berriolo-Riedinger A, Humbert O, Toubeau M, et al. In newly diagnosed diffuse large B-cell lymphoma, determination of bone marrow involvement with 18F-FDG PET/CT provides better diagnostic performance and prognostic stratification than does biopsy. J Nucl Med. 2013;54(8):1244-50.
69. Khan AB, Barrington SF, Mikhaeel NG, Hunt AA, Cameron L, Morris T, et al. PET-CT staging of DLBCL accurately identifies and provides new insight into the clinical significance of bone marrow involvement. Blood. 2013;122(1):61-7.
70. Frood R, Burton C, Tsoumpas C, Frangi AF, Gleeson F, Patel C, et al. Baseline PET/CT imaging parameters for prediction of treatment outcome in Hodgkin and diffuse large B cell lymphoma: a systematic review. Eur J Nucl Med Mol Imaging. 2021;48(10):3198-220.
71. Kwon SH, Kang DR, Kim J, Yoon JK, Lee SJ, Jeong SH, et al. Prognostic value of negative interim 2-[^{18}F]-fluoro-2-deoxy-d-glucose PET/CT in diffuse large B-cell lymphoma. Clin Radiol. 2016;71(3):280-6.
72. Gallicchio R, Mansueto G, Simeon V, Nardelli A, Guariglia R, Capacchione D, et al. F-18 FDG PET/CT quantization parameters as predictors of outcome in patients with diffuse large B-cell lymphoma. Eur J Haematol. 2014;92(5):382-9.
73. Miyazaki Y, Nawa Y, Miyagawa M, Kohashi S, Nakase K, Yasukawa M, et al. Maximum standard uptake value of 18F-fluorodeoxyglucose positron emission tomography is a prognostic factor for progression-free survival of newly diagnosed patients with diffuse large B cell lymphoma. Ann Hematol. 2013;92(2):239-44.
74. Ceriani L, Gritti G, Cascione L, Pirosa MC, Polino A, Ruberto T, et al. SAKK38/07 study: integration of baseline metabolic heterogeneity and metabolic tumor volume in DLBCL prognostic model. Blood Adv. 2020;4(6):1082-92.

75. Huang H, Xiao F, Han X, Zhong L, Zhong H, Xu L, et al. Correlation of pretreatment 18F-FDG uptake with clinicopathological factors and prognosis in patients with newly diagnosed diffuse large B-cell lymphoma. Nucl Med Commun. 2016;37(7):689-98.

76. Ilyas H, Mikhaeel NG, Dunn JT, Rahman F, Møller H, Smith D, et al. Defining the optimal method for measuring baseline metabolic tumour volume in diffuse large B cell lymphoma. Eur J Nucl Med Mol Imaging. 2018;45(7):1142-54.

77. Burggraaff CN, Rahman F, Kaßner I, Pieplenbosch S, Barrington SF, Jauw YWS, et al. Optimizing Workflows for Fast and Reliable Metabolic Tumor Volume Measurements in Diffuse Large B Cell Lymphoma. Mol Imaging Biol. 2020;22(4):1102-10.

78. Barrington SF, Meignan M. Time to Prepare for Risk Adaptation in Lymphoma by Standardizing Measurement of Metabolic Tumor Burden. J Nucl Med. 2019;60(8):1096-102.

79. Zsoter N, Bandi P, Szabo G, Toth Z, Bundschuh RA, Dinges J, et al. PET-CT based automated lung nodule detection. Annu Int Conf IEEE Eng Med Biol Soc. 2012;2012:4974-7.

80. Tan S, Li L, Choi W, Kang MK, D'Souza WD, Lu W. Adaptive region-growing with maximum curvature strategy for tumor segmentation in ^{18}F-FDG PET. Phys Med Biol. 2017;62(13):5383-402.

81. Barrington SF, Zwezerijnen BGJC, de Vet HCW, Heymans MW, Mikhaeel NG, Burggraaff CN, et al. Automated Segmentation of Baseline Metabolic Total Tumor Burden in Diffuse Large B-Cell Lymphoma: Which Method Is Most Successful? A Study on Behalf of the PETRA Consortium. J Nucl Med. 2021;62(3):332-7.

82. Jemaa S, Paulson JN, Hutchings M, Kostakoglu L, Trotman J, Tracy S, et al. Full automation of total metabolic tumor volume from FDG-PET/CT in DLBCL for baseline risk assessments. Cancer Imaging. 2022;22(1):39.

83. Guo B, Tan X, Ke Q, Cen H. Prognostic value of baseline metabolic tumor volume and total lesion glycolysis in patients with lymphoma: A meta-analysis. PLoS One. 2019;14(1):e0210224.

84. Mikhaeel NG, Heymans MW, Eertink JJ, de Vet HCW, Boellaard R, Dührsen U, et al. Proposed New Dynamic Prognostic Index for Diffuse Large B-Cell Lymphoma: International Metabolic Prognostic Index. J Clin Oncol. 2022:JCO2102063.

85. Xie M, Wu K, Liu Y, Jiang Q, Xie Y. Predictive value of F-18 FDG PET/CT quantization parameters in diffuse large B cell lymphoma: a meta-analysis with 702 participants. Med Oncol. 2015;32(1):446.

86. Islam P, Goldstein J, Flowers CR. PET-derived tumor metrics predict DLBCL response and progression-free survival. Leuk Lymphoma. 2019;60(8):1965-71.

87. Terasawa T, Nihashi T, Hotta T, Nagai H. 18F-FDG PET for posttherapy assessment of Hodgkin's disease and aggressive Non-Hodgkin's lymphoma: a systematic review. J Nucl Med. 2008;49(1):13-21.

88. Mikhaeel NG, Timothy AR, O'Doherty MJ, Hain S, Maisey MN. 18-FDG-PET as a prognostic indicator in the treatment of aggressive Non-Hodgkin's Lymphoma-comparison with CT. Leuk Lymphoma. 2000;39(5-6):543-53.

89. Spaepen K, Stroobants S, Dupont P, Van Steenweghen S, Thomas J, Vandenberghe P, et al. Prognostic value of positron emission tomography (PET) with fluorine-18 fluorodeoxyglucose ([18F]FDG) after first-line chemotherapy in non-Hodgkin's lymphoma: is [18F]FDG-PET a valid alternative to conventional diagnostic methods? J Clin Oncol. 2001;19(2):414-9.

90. Yang DH, Min JJ, Song HC, Jeong YY, Chung WK, Bae SY, et al. Prognostic significance of interim ^{18}F-FDG PET/CT after three or four cycles of R-CHOP chemotherapy in the treatment of diffuse large B-cell lymphoma. Eur J Cancer. 2011;47(9):1312-8.

91. Zinzani PL, Gandolfi L, Broccoli A, Argnani L, Fanti S, Pellegrini C, et al. Midtreatment 18F-fluorodeoxyglucose positron-emission tomography in aggressive non-Hodgkin lymphoma. Cancer. 2011;117(5):1010-8.

92. Safar V, Dupuis J, Itti E, Jardin F, Fruchart C, Bardet S, et al. Interim [18F]fluorodeoxyglucose positron emission tomography scan in diffuse large B-cell lymphoma treated with anthracycline-based chemotherapy plus rituximab. J Clin Oncol. 2012;30(2):184-90.

93. Haioun C, Itti E, Rahmouni A, Brice P, Rain JD, Belhadj K, et al. [18F]fluoro-2-deoxy-D-glucose positron emission tomography (FDG-PET) in aggressive lymphoma: an early prognostic tool for predicting patient outcome. Blood. 2005;106(4):1376-81.
94. Mikhaeel NG, Hutchings M, Fields PA, O'Doherty MJ, Timothy AR. FDG-PET after two to three cycles of chemotherapy predicts progression-free and overall survival in high-grade non-Hodgkin lymphoma. Ann Oncol. 2005;16(9):1514-23.
95. Eertink JJ, Burggraaff CN, Heymans MW, Dührsen U, Hüttmann A, Schmitz C, et al. Optimal timing and criteria of interim PET in DLBCL: a comparative study of 1692 patients. Blood Adv. 2021;5(9):2375-84.
96. Gallamini A, Zwarthoed C. Interim FDG-PET Imaging in Lymphoma. Semin Nucl Med. 2018;48(1):17-27.
97. Engles JM, Quarless SA, Mambo E, Ishimori T, Cho SY, Wahl RL. Stunning and its effect on 3H-FDG uptake and key gene expression in breast cancer cells undergoing chemotherapy. J Nucl Med. 2006;47(4):603-8.
98. Spaepen K, Stroobants S, Dupont P, Bormans G, Balzarini J, Verhoef G, et al. [(18)F]FDG PET monitoring of tumour response to chemotherapy: does [(18)F]FDG uptake correlate with the viable tumour cell fraction? Eur J Nucl Med Mol Imaging. 2003;30(5):682-8.
99. Burggraaff CN, de Jong A, Hoekstra OS, Hoetjes NJ, Nievelstein RAJ, Jansma EP, et al. Predictive value of interim positron emission tomography in diffuse large B-cell lymphoma: a systematic review and meta-analysis. Eur J Nucl Med Mol Imaging. 2019;46(1):65-79.
100. Fan Y, Zhang Y, Yang Z, Ying Z, Zhou N, Liu C, et al. Evaluating early interim fluorine-18 fluorodeoxyglucose positron emission tomography/computed tomography with the $SUV_{max\text{-}liver}$-based interpretation for predicting the outcome in diffuse large B-cell lymphoma. Leuk Lymphoma. 2017;58(9):1-9.
101. Kim J, Lee JO, Paik JH, Lee WW, Kim SE, Song YS. Different predictive values of interim ^{18}F-FDG PET/CT in germinal center like and non-germinal center like diffuse large B-cell lymphoma. Ann Nucl Med. 2017;31(1):1-11.
102. Mikhaeel NG, Smith D, Dunn JT, Phillips M, Møller H, Fields PA, et al. Combination of baseline metabolic tumour volume and early response on PET/CT

improves progression-free survival prediction in DLBCL. Eur J Nucl Med Mol Imaging. 2016;43(7):1209-19.

103. Mamot C, Klingbiel D, Hitz F, Renner C, Pabst T, Driessen C, et al. Final Results of a Prospective Evaluation of the Predictive Value of Interim Positron Emission Tomography in Patients With Diffuse Large B-Cell Lymphoma Treated With R-CHOP-14 (SAKK 38/07). J Clin Oncol. 2015;33(23):2523-9.

104. Carr R, Fanti S, Paez D, Cerci J, Györke T, Redondo F, et al. Prospective international cohort study demonstrates inability of interim PET to predict treatment failure in diffuse large B-cell lymphoma. J Nucl Med. 2014;55(12):1936-44.

105. Fuertes S, Setoain X, Lopez-Guillermo A, Carrasco JL, Rodríguez S, Rovira J, et al. Interim FDG PET/CT as a prognostic factor in diffuse large B-cell lymphoma. Eur J Nucl Med Mol Imaging. 2013;40(4):496-504.

106. Itti E, Meignan M, Berriolo-Riedinger A, Biggi A, Cashen AF, Véra P, et al. An international confirmatory study of the prognostic value of early PET/CT in diffuse large B-cell lymphoma: comparison between Deauville criteria and ΔSUVmax. Eur J Nucl Med Mol Imaging. 2013;40(9):1312-20.

107. Barrington SF, Sulkin T, Forbes A, Johnson PWM. All that glitters is not gold - new reconstruction methods using Deauville criteria for patient reporting. Eur J Nucl Med Mol Imaging. 2018;45(2):316-7.

108. Lasnon C, Enilorac B, Aide N. Reply to: "All that glitters is not gold - new reconstruction methods using Deauville criteria for patient reporting". Eur J Nucl Med Mol Imaging. 2018;45(5):878-81.

109. Wyrzykowski M, Siminiak N, Kaźmierczak M, Ruchała M, Czepczyński R. Impact of the Q.Clear reconstruction algorithm on the interpretation of PET/CT images in patients with lymphoma. EJNMMI Res. 2020;10(1):99.

110. Lin C, Itti E, Haioun C, Petegnief Y, Luciani A, Dupuis J, et al. Early 18F-FDG PET for prediction of prognosis in patients with diffuse large B-cell lymphoma: SUV-based assessment versus visual analysis. J Nucl Med. 2007;48(10):1626-32.

111. Mikhaeel NG, Cunningham D, Counsell N, McMillan A, Radford JA, Ardeshna KM, et al. FDG-PET/CT after two cycles of R-CHOP in DLBCL predicts complete remission but has limited value in identifying patients with poor outcome - final result of

a UK National Cancer Research Institute prospective study. Br J Haematol. 2021;192(3):504-13.

112. Schöder H, Polley MC, Knopp MV, Hall N, Kostakoglu L, Zhang J, et al. Prognostic value of interim FDG-PET in diffuse large cell lymphoma: results from the CALGB 50303 Clinical Trial. Blood. 2020;135(25):2224-34.

113. Rekowski J, Hüttmann A, Schmitz C, Müller SP, Kurch L, Kotzerke J, et al. Interim PET Evaluation in Diffuse Large B-Cell Lymphoma Using Published Recommendations: Comparison of the Deauville 5-Point Scale and the ΔSUV. J Nucl Med. 2021;62(1):37-42.

114. Burggraaff CN, Eertink JJ, Lugtenburg PJ, Hoekstra OS, Arens AIJ, de Keizer B, et al. ^{18}F-FDG PET improves baseline clinical predictors of response in diffuse large B-cell lymphoma: The HOVON-84 study. J Nucl Med. 2021.

115. Hasenclever D, Kurch L, Mauz-Körholz C, Elsner A, Georgi T, Wallace H, et al. qPET - a quantitative extension of the Deauville scale to assess response in interim FDG-PET scans in lymphoma. Eur J Nucl Med Mol Imaging. 2014;41(7):1301-8.

116. Mauz-Körholz C, Landman-Parker J, Balwierz W, Ammann RA, Anderson RA, Attarbaschi A, et al. Response-adapted omission of radiotherapy and comparison of consolidation chemotherapy in children and adolescents with intermediate-stage and advanced-stage classical Hodgkin lymphoma (EuroNet-PHL-C1): a titration study with an open-label, embedded, multinational, non-inferiority, randomised controlled trial. Lancet Oncol. 2022;23(1):125-37.

117. Kurch L, Hasenclever D, Kluge R, Georgi T, Tchavdarova L, Golombeck M, et al. Only strongly enhanced residual FDG uptake in early response PET (Deauville 5 or qPET ≥ 2) is prognostic in pediatric Hodgkin lymphoma: Results of the GPOH-HD2002 trial. Pediatr Blood Cancer. 2019;66(3):e27539.

118. Georgi TW, Kurch L, Hasenclever D, Warbey VS, Pike L, Radford J, et al. Quantitative assessment of interim PET in Hodgkin lymphoma: An evaluation of the qPET method in adult patients in the RAPID trial. PLoS One. 2020;15(4):e0231027.

119. Kurch L, Hüttmann A, Georgi TW, Rekowski J, Sabri O, Schmitz C, et al. Interim PET in Diffuse Large B-Cell Lymphoma. J Nucl Med. 2021;62(8):1068-74.

120. Annunziata S, Cuccaro A, Calcagni ML, Hohaus S, Giordano A, Rufini V. Interim FDG-PET/CT in Hodgkin lymphoma: the prognostic role of the ratio between target lesion and liver SUVmax (rPET). Ann Nucl Med. 2016;30(8):588-92.
121. Toledano MN, Vera P, Tilly H, Jardin F, Becker S. Comparison of therapeutic evaluation criteria in FDG-PET/CT in patients with diffuse large-cell B-cell lymphoma: Prognostic impact of tumor/liver ratio. PLoS One. 2019;14(2):e0211649.
122. Barrington SF, Kluge R. FDG PET for therapy monitoring in Hodgkin and non-Hodgkin lymphomas. Eur J Nucl Med Mol Imaging. 2017;44(Suppl 1):97-110.
123. Weber WA. Use of PET for monitoring cancer therapy and for predicting outcome. J Nucl Med. 2005;46(6):983-95.
124. Geworski L, Knoop BO, de Cabrejas ML, Knapp WH, Munz DL. Recovery correction for quantitation in emission tomography: a feasibility study. Eur J Nucl Med. 2000;27(2):161-9.
125. Kuhnert G, Boellaard R, Sterzer S, Kahraman D, Scheffler M, Wolf J, et al. Impact of PET/CT image reconstruction methods and liver uptake normalization strategies on quantitative image analysis. Eur J Nucl Med Mol Imaging. 2016;43(2):249-58.
126. Quak E, Hovhannisyan N, Lasnon C, Fruchart C, Vilque JP, Musafiri D, et al. The importance of harmonizing interim positron emission tomography in non-Hodgkin lymphoma: focus on the Deauville criteria. Haematologica. 2014;99(6):e84-5.
127. Genc M, Yildirim N, Coskun N, Ozdemir E, Turkolmez S. The variation of quantitative parameters and Deauville scores with different reconstruction algorithms in FDG PET/CT imaging of lymphoma patients. Rev Esp Med Nucl Imagen Mol (Engl Ed). 2023;42(6):388-92.
128. Mayerhoefer ME, Materka A, Langs G, Häggström I, Szczypiński P, Gibbs P, et al. Introduction to Radiomics. J Nucl Med. 2020;61(4):488-95.
129. Yip SS, Aerts HJ. Applications and limitations of radiomics. Phys Med Biol. 2016;61(13):R150-66.
130. Gillies RJ, Kinahan PE, Hricak H. Radiomics: Images Are More than Pictures, They Are Data. Radiology. 2016;278(2):563-77.
131. Sutton RN, Hall EL. Texture Measures for Automatic Classification of Pulmonary Disease. IEEE Transactions on Computers. 1972;C21:667 - 76.

132. Lambin P, Rios-Velazquez E, Leijenaar R, Carvalho S, van Stiphout RG, Granton P, et al. Radiomics: extracting more information from medical images using advanced feature analysis. Eur J Cancer. 2012;48(4):441-6.
133. Morris LG, Riaz N, Desrichard A, Şenbabaoğlu Y, Hakimi AA, Makarov V, et al. Pan-cancer analysis of intratumor heterogeneity as a prognostic determinant of survival. Oncotarget. 2016;7(9):10051-63.
134. Orlhac F, Nioche C, Klyuzhin I, Rahmim A, Buvat I. Radiomics in PET Imaging:: A Practical Guide for Newcomers. PET Clin. 2021;16(4):597-612.
135. Ha S, Choi H, Paeng JC, Cheon GJ. Radiomics in Oncological PET/CT: a Methodological Overview. Nucl Med Mol Imaging. 2019;53(1):14-29.
136. Castellano G, Bonilha L, Li LM, Cendes F. Texture analysis of medical images. Clin Radiol. 2004;59(12):1061-9.
137. Chicklore S, Goh V, Siddique M, Roy A, Marsden PK, Cook GJ. Quantifying tumour heterogeneity in 18F-FDG PET/CT imaging by texture analysis. Eur J Nucl Med Mol Imaging. 2013;40(1):133-40.
138. Galloway MM. Texture analysis using gray level run lengths. Computer Graphics and Image Processing. 1975;4(2):172-9.
139. Thibault G, Angulo J, Meyer F. Advanced statistical matrices for texture characterization: application to cell classification. IEEE Trans Biomed Eng. 2014;61(3):630-7.
140. Jiang H, Li A, Ji Z, Tian M, Zhang H. Role of Radiomics-Based Baseline PET/CT Imaging in Lymphoma: Diagnosis, Prognosis, and Response Assessment. Mol Imaging Biol. 2022;24(4):537-49.
141. Parvez A, Tau N, Hussey D, Maganti M, Metser U. F-FDG PET/CT metabolic tumor parameters and radiomics features in aggressive non-Hodgkin's lymphoma as predictors of treatment outcome and survival. Ann Nucl Med. 2018;32(6):410-6.
142. Aide N, Talbot M, Fruchart C, Damaj G, Lasnon C. Diagnostic and prognostic value of baseline FDG PET/CT skeletal textural features in diffuse large B cell lymphoma. Eur J Nucl Med Mol Imaging. 2018;45(5):699-711.
143. Zhou Y, Ma XL, Pu LT, Zhou RF, Ou XJ, Tian R. Prediction of Overall Survival and Progression-Free Survival by the ^{18}F-FDG PET/CT Radiomic Features in Patients

with Primary Gastric Diffuse Large B-Cell Lymphoma. Contrast Media Mol Imaging. 2019;2019:5963607.

144. Aide N, Fruchart C, Nganoa C, Gac AC, Lasnon C. Baseline ^{18}F-FDG PET radiomic features as predictors of 2-year event-free survival in diffuse large B cell lymphomas treated with immunochemotherapy. Eur Radiol. 2020;30(8):4623-32.

145. Sun Y, Qiao X, Jiang C, Liu S, Zhou Z. Texture Analysis Improves the Value of Pretreatment ^{18}F-FDG PET/CT in Predicting Interim Response of Primary Gastrointestinal Diffuse Large B-Cell Lymphoma. Contrast Media Mol Imaging. 2020;2020:2981585.

146. Lue KH, Wu YF, Lin HH, Hsieh TC, Liu SH, Chan SC, et al. Prognostic Value of Baseline Radiomic Features of ^{18}F-FDG PET in Patients with Diffuse Large B-Cell Lymphoma. Diagnostics (Basel). 2020;11(1).

147. Cottereau AS, Nioche C, Dirand AS, Clerc J, Morschhauser F, Casasnovas O, et al. F-FDG PET Dissemination Features in Diffuse Large B-Cell Lymphoma Are Predictive of Outcome. J Nucl Med. 2020;61(1):40-5.

148. Coskun N, Okudan B, Uncu D, Kitapci MT. Baseline 18F-FDG PET textural features as predictors of response to chemotherapy in diffuse large B-cell lymphoma. Nucl Med Commun. 2021;42(11):1227-32.

149. Ritter Z, Papp L, Zámbó K, Tóth Z, Dezső D, Veres DS, et al. Two-Year Event-Free Survival Prediction in DLBCL Patients Based on *In Vivo* Radiomics and Clinical Parameters. Front Oncol. 2022;12:820136.

150. Eertink JJ, van de Brug T, Wiegers SE, Zwezerijnen GJC, Pfaehler EAG, Lugtenburg PJ, et al. ^{18}F-FDG PET baseline radiomics features improve the prediction of treatment outcome in diffuse large B-cell lymphoma. Eur J Nucl Med Mol Imaging. 2022;49(3):932-42.

151. Cui Y, Jiang Y, Deng X, Long W, Liu B, Fan W, et al. 18F-FDG PET-Based Combined Baseline and End-Of-Treatment Radiomics Model Improves the Prognosis Prediction in Diffuse Large B Cell Lymphoma After First-Line Therapy. Acad Radiol. 2023;30(7):1408-18.

152. Jing F, Liu Y, Zhao X, Wang N, Dai M, Chen X, et al. Baseline ^{18}F-FDG PET/CT radiomics for prognosis prediction in diffuse large B cell lymphoma. EJNMMI Res. 2023;13(1):92.

153. Li M, Yao H, Zhang P, Zhang L, Liu W, Jiang Z, et al. Development and validation of a [^{18}F]FDG PET/CT-based radiomics nomogram to predict the prognostic risk of pretreatment diffuse large B cell lymphoma patients. Eur Radiol. 2023;33(5):3354-65.
154. Eertink JJ, Zwezerijnen GJC, Heymans MW, Pieplenbosch S, Wiegers SE, Dührsen U, et al. Baseline PET radiomics outperforms the IPI risk score for prediction of outcome in diffuse large B-cell lymphoma. Blood. 2023;141(25):3055-64.
155. Czibor S, Carr R, Redondo F, Auewarakul CU, Cerci JJ, Paez D, et al. Prognostic parameters on baseline and interim [18F]FDG-PET/computed tomography in diffuse large B-cell lymphoma patients. Nucl Med Commun. 2023;44(4):291-301.
156. Czibor S, Csatlós Z, Fábián K, Piroska M, Györke T. Volumetric and textural analysis of PET/CT in patients with diffuse large B-cell lymphoma highlights the importance of novel MTVrate feature. Nucl Med Commun. 2024.
157. Zhuang M, García DV, Kramer GM, Frings V, Smit EF, Dierckx R, et al. Variability and Repeatability of Quantitative Uptake Metrics in ^{18} F-FDG PET/CT of Non-Small Cell Lung Cancer: Impact of Segmentation Method, Uptake Interval, and Reconstruction Protocol. J Nucl Med. 2019;60(5):600-7.
158. Tutino F, Puccini G, Linguanti F, Puccini B, Rigacci L, Kovalchuk S, et al. Baseline metabolic tumor volume calculation using different SUV thresholding methods in Hodgkin lymphoma patients: interobserver agreement and reproducibility across software platforms. Nucl Med Commun. 2021;42(3):284-91.
159. Kanoun S, Tal I, Berriolo-Riedinger A, Rossi C, Riedinger JM, Vrigneaud JM, et al. Influence of Software Tool and Methodological Aspects of Total Metabolic Tumor Volume Calculation on Baseline [18F]FDG PET to Predict Survival in Hodgkin Lymphoma. PLoS One. 2015;10(10):e0140830.
160. Hutchings M, Loft A, Hansen M, Ralfkiaer E, Specht L. Different histopathological subtypes of Hodgkin lymphoma show significantly different levels of FDG uptake. Hematol Oncol. 2006;24(3):146-50.
161. Boktor RR, Walker G, Stacey R, Gledhill S, Pitman AG. Reference range for intrapatient variability in blood-pool and liver SUV for 18F-FDG PET. J Nucl Med. 2013;54(5):677-82.
162. Sasanelli M, Meignan M, Haioun C, Berriolo-Riedinger A, Casasnovas RO, Biggi A, et al. Pretherapy metabolic tumour volume is an independent predictor of outcome in

patients with diffuse large B-cell lymphoma. Eur J Nucl Med Mol Imaging. 2014;41(11):2017-22.

163. Chang CC, Cho SF, Chuang YW, Lin CY, Chang SM, Hsu WL, et al. Prognostic significance of total metabolic tumor volume on ^{18}F-fluorodeoxyglucose positron emission tomography/ computed tomography in patients with diffuse large B-cell lymphoma receiving rituximab-containing chemotherapy. Oncotarget. 2017;8(59):99587-600.

164. Oh MY, Chung JS, Song MK, Shin HJ, Lee HS, Lee SM, et al. Prognostic value of Waldeyer's ring involvement of diffuse large B-cell lymphoma treated with R-CHOP. Int J Hematol. 2013;97(3):397-402.

165. Song MK, Yang DH, Lee GW, Lim SN, Shin S, Pak KJ, et al. High total metabolic tumor volume in PET/CT predicts worse prognosis in diffuse large B cell lymphoma patients with bone marrow involvement in rituximab era. Leuk Res. 2016;42:1-6.

166. Toledano MN, Desbordes P, Banjar A, Gardin I, Vera P, Ruminy P, et al. Combination of baseline FDG PET/CT total metabolic tumour volume and gene expression profile have a robust predictive value in patients with diffuse large B-cell lymphoma. Eur J Nucl Med Mol Imaging. 2018;45(5):680-8.

167. Adams HJ, Nievelstein RA, Kwee TC. Prognostic value of complete remission status at end-of-treatment FDG-PET in R-CHOP-treated diffuse large B-cell lymphoma: systematic review and meta-analysis. Br J Haematol. 2015;170(2):185-91.

168. Ding CY, Guo Z, Sun J, Yang WP, Li TR. [Prognostic value of pretreatment (18)F-FDG PET-CT for patients with advanced diffuse large B-cell lymphoma]. Zhonghua Zhong Liu Za Zhi. 2018;40(7):528-33.

169. Dührsen U, Müller S, Hertenstein B, Thomssen H, Kotzerke J, Mesters R, et al. Positron Emission Tomography-Guided Therapy of Aggressive Non-Hodgkin Lymphomas (PETAL): A Multicenter, Randomized Phase III Trial. J Clin Oncol. 2018;36(20):2024-34.

170. Casasnovas RO, Ysebaert L, Thieblemont C, Bachy E, Feugier P, Delmer A, et al. FDG-PET-driven consolidation strategy in diffuse large B-cell lymphoma: final results of a randomized phase 2 study. Blood. 2017;130(11):1315-26.

171. Laffon E, Marthan R. FDG PET for therapy monitoring in Hodgkin's and non-Hodgkin's lymphomas: qPET versus rPET. Eur J Nucl Med Mol Imaging. 2017;44(9):1602-3.
172. Gallamini A, Barrington SF, Biggi A, Chauvie S, Kostakoglu L, Gregianin M, et al. The predictive role of interim positron emission tomography for Hodgkin lymphoma treatment outcome is confirmed using the interpretation criteria of the Deauville five-point scale. Haematologica. 2014;99(6):1107-13.
173. Poeschel V, Held G, Ziepert M, Witzens-Harig M, Holte H, Thurner L, et al. Four versus six cycles of CHOP chemotherapy in combination with six applications of rituximab in patients with aggressive B-cell lymphoma with favourable prognosis (FLYER): a randomised, phase 3, non-inferiority trial. Lancet. 2019;394(10216):2271-81.
174. van Velden FH, Kramer GM, Frings V, Nissen IA, Mulder ER, de Langen AJ, et al. Repeatability of Radiomic Features in Non-Small-Cell Lung Cancer [(18)F]FDG-PET/CT Studies: Impact of Reconstruction and Delineation. Mol Imaging Biol. 2016;18(5):788-95.
175. Cook GJR, Goh V. A Role for FDG PET Radiomics in Personalized Medicine? Semin Nucl Med. 2020;50(6):532-40.
176. Sehn LH, Salles G. Diffuse Large B-Cell Lymphoma. N Engl J Med. 2021;384(9):842-58.

9. BIBLIOGRAPHY OF THE CANDIDATE'S PUBLICATIONS

Publications related to the thesis:

Czibor S, Carr R, Redondo F, Auewarakul CU, Cerci JJ, Paez D, Fanti S, Györke T. (2023) Prognostic parameters on baseline and interim [18F]FDG-PET/computed tomography in diffuse large B-cell lymphoma patients. Nucl Med Commun, 44: 291-301.

IF: 1.3

Czibor S, Csatlós Z, Fábián K, Piroska M, Györke T. (2024) Volumetric and textural analysis of PET/CT in patients with diffuse large B-cell lymphoma highlights the importance of novel MTVrate feature. Nucl Med Commun, 45: 931-937.

IF: 1.3 (2023)

∑IF: 2.6

Publications not related to the thesis:

Czibor S, Bibok A, Horváthy D, Fábián K, Györke T. (2023) Radioembolization Planning With Dual-Isotope Acquisition of ^{166}Ho-Labeled Microparticles and ^{99m}Tc-Mebrofenin. Clin Nucl Med, 48: 719-721.

Czibor S, Kristóf E, Kecskés K, Barra M, Szántó P, Maurovich-Horvat P, Györke T. (2020) Oncologic patient with COVID-19 discovered incidentally by PET/CT examination: (A COVID–19-pandémia orvosszakmai kérdései). Orv Hetil, 161: 971-976. [Hungarian]

IF: 0.54

Jorgov L, Magyar B, Piroska M, **Czibor S**, Györke T. (2024) Brown adipose tissue activation in paediatric and adolescent oncological (Hodgkin lymphoma or sarcoma) cases visualised on FDG PET/CT. Imaging, doi:10.1556/1647.2024.00262.

IF: 0.7 (2023)

Bibok A, Sólymos P, **Czibor S**, Korda DA, Nádasdy-Horváth D, Demeter G, Taba G, Deak PA, Horváthy DB. (2024) Closed System Injection of Two Separate Vials of 166 Holmium-Labeled Microspheres in a Large Hepatocellular Carcinoma. Cardiovasc Intervent Radiol, doi:10.1007/s00270-024-03878-8.

Ferrández MC, Golla SSV, Eertink JJ, Wiegers SE, Zwezerijnen GJC, Heymans MW, Lugtenburg PJ, Kurch L, Hüttmann A, Hanoun C, Dührsen U, Barrington SF, Mikhaeel NG, Ceriani L, Zucca E, **Czibor S**, Györke T, Chamuleau MED, Zijlstra JM, Boellaard R, PETRA Consortium. (2024) Validation of an Artificial Intelligence-Based Prediction Model Using 5 External PET/CT Datasets of Diffuse Large B-Cell Lymphoma. J Nucl Med, 65: 1802-1807.

IF: 9.1 (2023)

Eertink JJ, Zwezerijnen GJC, Heymans MW, Pieplenbosch S, Wiegers SE, Dührsen U, Hüttmann A, Kurch L, Hanoun C, Lugtenburg PJ, Barrington SF, Mikhaeel NG, Ceriani L, Zucca E, **Czibor S**, Györke T, Chamuleau MED, Hoekstra OS, de Vet HCW, Boellaard R, Zijlstra JM. (2023) Baseline PET radiomics outperforms the IPI risk score for prediction of outcome in diffuse large B-cell lymphoma. Blood, 141: 3055-3064.

IF: 21.1

Milecz-Mitykó R, Bérczi V, **Czibor S**, Bánsághi Z, Taba G, Kári B, Györke T. (2023) Preliminary study on individual radiation dose received by medical staff for dose constraint determination. Radiat Prot Dosimetry, 199: 989-994.

IF: 0.8

Eertink JJ, Burggraaff CN, Heymans MW, Dührsen U, Hüttmann A, Schmitz C, Müller S, Lugtenburg PJ, Barrington SF, Mikhaeel NG, Carr R, **Czibor S**, Györke T, Ceriani L, Zucca E, Hutchings M, Kostakoglu L, Loft A, Fanti S, Wiegers SE, Pieplenbosch S, Boellaard R, Hoekstra OS, Zijlstra JM, de Vet HCW. (2021) Optimal timing and criteria of interim PET in DLBCL: a comparative study of 1692 patients. Blood Adv, 5: 2375-2384.

IF: 7.642

Peskó G, Jenei Z, Varga G, Apor A, Vágó H, **Czibor S**, Prohászka Z, Masszi T, Pozsonyi Z. (2019) Coexistence of aortic valve stenosis and cardiac amyloidosis: echocardiographic and clinical significance. Cardiovasc Ultrasound, 17: 32.

IF: 2.051

∑IF: 41.933

10. ACKNOWLEDGEMENTS

Thank you to my supervisor, Dr Tamás Györke, for providing guidance and feedback throughout this project.

It would take another dissertation to properly express my gratitude towards my wife, Dr Nikolett Marton. I am truly honoured to have her by my side.

This thesis is a reflection of the unwavering support and boundless love I received from my family and friends during this challenging academic pursuit. I owe an immense debt of gratitude to my parents and my sister, who nurtured my curiosity and supported my educational endeavours from the very beginning.

My appreciation also goes to the staff at the Medical Imaging Centre at Semmelweis University and Pozitron Medical Diagnostics Ltd. whose resources and assistance have been invaluable.

I am grateful for the insights gathered from the participation in PETRA Consortium projects.

My sincere thanks to those graduate students who trusted me to supervise their scientific work.

The Workgroup for Science Management of the Doctoral College at Semmelweis University provided valuable help for this dissertation and I am grateful for their support.